

Resonant structure of $\tau \rightarrow 3\pi\pi^0\nu_\tau$ and $\tau \rightarrow \omega\pi\nu_\tau$ decays

CLEO Collaboration

(September 17, 2018)

Abstract

The resonant structure of the four pion final state in the decay $\tau \rightarrow 3\pi\pi^0\nu_\tau$ is analyzed using 4.27 million $\tau^+\tau^-$ pairs collected by the CLEO II experiment. We search for second class currents in the decay $\tau \rightarrow \omega\pi\nu_\tau$ using spin-parity analysis and establish an upper limit on the non-vector current contribution. The mass and width of the ρ' resonance are extracted from a fit to the $\tau \rightarrow \omega\pi\nu_\tau$ spectral function. A partial wave analysis of the resonant structure of the $\tau \rightarrow 3\pi\pi^0\nu_\tau$ decay is performed; the spectral decomposition of the four pion system is dominated by the $\omega\pi$ and $a_1\pi$ final states.

K. W. Edwards,¹ R. Janicek,² P. M. Patel,² A. J. Sadoff,³ R. Ammar,⁴ P. Baringer,⁴
 A. Bean,⁴ D. Besson,⁴ R. Davis,⁴ S. Kotov,⁴ I. Kravchenko,⁴ N. Kwak,⁴ X. Zhao,⁴
 S. Anderson,⁵ V. V. Frolov,⁵ Y. Kubota,⁵ S. J. Lee,⁵ R. Mahapatra,⁵ J. J. O'Neill,⁵
 R. Poling,⁵ T. Riehle,⁵ A. Smith,⁵ S. Ahmed,⁶ M. S. Alam,⁶ S. B. Athar,⁶ L. Jian,⁶
 L. Ling,⁶ A. H. Mahmood,^{6,*} M. Saleem,⁶ S. Timm,⁶ F. Wappler,⁶ A. Anastassov,⁷
 J. E. Duboscq,⁷ K. K. Gan,⁷ C. Gwon,⁷ T. Hart,⁷ K. Honscheid,⁷ H. Kagan,⁷ R. Kass,⁷
 J. Lorenc,⁷ H. Schwarthoff,⁷ E. von Toerne,⁷ M. M. Zoeller,⁷ S. J. Richichi,⁸ H. Severini,⁸
 P. Skubic,⁸ A. Undrus,⁸ M. Bishai,⁹ S. Chen,⁹ J. Fast,⁹ J. W. Hinson,⁹ J. Lee,⁹ N. Menon,⁹
 D. H. Miller,⁹ E. I. Shibata,⁹ I. P. J. Shipsey,⁹ Y. Kwon,^{10,†} A.L. Lyon,¹⁰
 E. H. Thorndike,¹⁰ C. P. Jessop,¹¹ K. Lingel,¹¹ H. Marsiske,¹¹ M. L. Perl,¹¹ V. Savinov,¹¹
 D. Ugolini,¹¹ X. Zhou,¹¹ T. E. Coan,¹² V. Fadeyev,¹² I. Korolkov,¹² Y. Maravin,¹²
 I. Narsky,¹² V. Shelkov,¹² R. Stroynowski,¹² J. Ye,¹² T. Wlodek,¹² M. Artuso,¹³ R. Ayad,¹³
 E. Dambasuren,¹³ S. Kopp,¹³ G. Majumder,¹³ G. C. Moneti,¹³ R. Mountain,¹³ S. Schuh,¹³
 T. Skwarnicki,¹³ S. Stone,¹³ A. Titov,¹³ G. Viehhauser,¹³ J.C. Wang,¹³ A. Wolf,¹³ J. Wu,¹³
 S. E. Csorna,¹⁴ K. W. McLean,¹⁴ S. Marka,¹⁴ Z. Xu,¹⁴ R. Godang,¹⁵ K. Kinoshita,^{15,‡}
 I. C. Lai,¹⁵ P. Pomianowski,¹⁵ S. Schrenk,¹⁵ G. Bonvicini,¹⁶ D. Cinabro,¹⁶ R. Greene,¹⁶
 L. P. Perera,¹⁶ G. J. Zhou,¹⁶ S. Chan,¹⁷ G. Eigen,¹⁷ E. Lipeles,¹⁷ M. Schmidtler,¹⁷
 A. Shapiro,¹⁷ W. M. Sun,¹⁷ J. Urheim,¹⁷ A. J. Weinstein,¹⁷ F. Würthwein,¹⁷ D. E. Jaffe,¹⁸
 G. Masek,¹⁸ H. P. Paar,¹⁸ E. M. Potter,¹⁸ S. Prell,¹⁸ V. Sharma,¹⁸ D. M. Asner,¹⁹
 A. Eppich,¹⁹ J. Gronberg,¹⁹ T. S. Hill,¹⁹ D. J. Lange,¹⁹ R. J. Morrison,¹⁹ T. K. Nelson,¹⁹
 J. D. Richman,¹⁹ R. A. Briere,²⁰ B. H. Behrens,²¹ W. T. Ford,²¹ A. Gritsan,²¹ H. Krieg,²¹
 J. Roy,²¹ J. G. Smith,²¹ J. P. Alexander,²² R. Baker,²² C. Bebek,²² B. E. Berger,²²
 K. Berkelman,²² F. Blanc,²² V. Boisvert,²² D. G. Cassel,²² M. Dickson,²² P. S. Drell,²²
 K. M. Ecklund,²² R. Ehrlich,²² A. D. Foland,²² P. Gaidarev,²² R. S. Galik,²² L. Gibbons,²²
 B. Gittelman,²² S. W. Gray,²² D. L. Hartill,²² B. K. Heltsley,²² P. I. Hopman,²²
 C. D. Jones,²² D. L. Kreinick,²² T. Lee,²² Y. Liu,²² T. O. Meyer,²² N. B. Mistry,²²
 C. R. Ng,²² E. Nordberg,²² J. R. Patterson,²² D. Peterson,²² D. Riley,²² J. G. Thayer,²²
 P. G. Thies,²² B. Valant-Spaight,²² A. Warburton,²² P. Avery,²³ M. Lohner,²³ C. Prescott,²³
 A. I. Rubiera,²³ J. Yelton,²³ J. Zheng,²³ G. Brandenburg,²⁴ A. Ershov,²⁴ Y. S. Gao,²⁴
 D. Y.-J. Kim,²⁴ R. Wilson,²⁴ T. E. Browder,²⁵ Y. Li,²⁵ J. L. Rodriguez,²⁵ H. Yamamoto,²⁵
 T. Bergfeld,²⁶ B. I. Eisenstein,²⁶ J. Ernst,²⁶ G. E. Gladding,²⁶ G. D. Gollin,²⁶
 R. M. Hans,²⁶ E. Johnson,²⁶ I. Karliner,²⁶ M. A. Marsh,²⁶ M. Palmer,²⁶ C. Plager,²⁶
 C. Sedlack,²⁶ M. Selen,²⁶ J. J. Thaler,²⁶ and J. Williams²⁶

¹Carleton University, Ottawa, Ontario, Canada K1S 5B6
and the Institute of Particle Physics, Canada

²McGill University, Montréal, Québec, Canada H3A 2T8
and the Institute of Particle Physics, Canada

*Permanent address: University of Texas - Pan American, Edinburg TX 78539.

†Permanent address: Yonsei University, Seoul 120-749, Korea.

‡Permanent address: University of Cincinnati, Cincinnati OH 45221

- ³Ithaca College, Ithaca, New York 14850
- ⁴University of Kansas, Lawrence, Kansas 66045
- ⁵University of Minnesota, Minneapolis, Minnesota 55455
- ⁶State University of New York at Albany, Albany, New York 12222
- ⁷Ohio State University, Columbus, Ohio 43210
- ⁸University of Oklahoma, Norman, Oklahoma 73019
- ⁹Purdue University, West Lafayette, Indiana 47907
- ¹⁰University of Rochester, Rochester, New York 14627
- ¹¹Stanford Linear Accelerator Center, Stanford University, Stanford, California 94309
- ¹²Southern Methodist University, Dallas, Texas 75275
- ¹³Syracuse University, Syracuse, New York 13244
- ¹⁴Vanderbilt University, Nashville, Tennessee 37235
- ¹⁵Virginia Polytechnic Institute and State University, Blacksburg, Virginia 24061
- ¹⁶Wayne State University, Detroit, Michigan 48202
- ¹⁷California Institute of Technology, Pasadena, California 91125
- ¹⁸University of California, San Diego, La Jolla, California 92093
- ¹⁹University of California, Santa Barbara, California 93106
- ²⁰Carnegie Mellon University, Pittsburgh, Pennsylvania 15213
- ²¹University of Colorado, Boulder, Colorado 80309-0390
- ²²Cornell University, Ithaca, New York 14853
- ²³University of Florida, Gainesville, Florida 32611
- ²⁴Harvard University, Cambridge, Massachusetts 02138
- ²⁵University of Hawaii at Manoa, Honolulu, Hawaii 96822
- ²⁶University of Illinois, Urbana-Champaign, Illinois 61801

I. INTRODUCTION

The resonant structure of the decay $\tau \rightarrow 4\pi\nu_\tau$ has been the subject of experimental studies for the past several decades. The first observations of $\tau \rightarrow \omega\pi\nu_\tau$ were reported by the ARGUS [1] and the CLEO [2] Collaborations in 1987. Since then, the ARGUS Collaboration estimated [3] the $\rho\pi\pi$ branching fractions and the ALEPH Collaboration provided improved measurements [4] of branching fractions of the $\tau \rightarrow 4\pi\nu_\tau$ subchannels. No attempt has been made, so far, to determine a complete resonant structure of the four pion final state.

In the Standard Model, τ decays to four pions proceed via vector current producing hadrons in the $J^P = 1^-$ spin-parity state. At low energies, the hadronic current is dominated by vector ρ , ρ' and ρ'' resonance form factors which can be approximated by relativistic Breit-Wigner functions. The full formalism is discussed in Refs. [5–8]. The parameters of $J^P = 1^-$ resonances are of particular interest for phenomenological tests of the Conserved Vector Current (CVC) hypothesis that compare multipion final states in τ decays and e^+e^- annihilations [9]. So far, there have been only two published attempts [10,11] to extract the mass and width of the ρ' resonance from analyses of the $\tau \rightarrow \pi\pi^0\nu_\tau$ decay and none from $\tau \rightarrow 4\pi\nu_\tau$.

In this study, we determine the resonant decomposition of the decay $\tau \rightarrow \omega\pi\nu_\tau$ and search for second class currents via a spin parity analysis. We fit the $\tau \rightarrow \omega\pi\nu_\tau$ spectral function to obtain the relative contributions of the ρ , ρ' and ρ'' resonances, as well as the mass and width of the ρ' meson. We assume that in a first approximation the widths of the ρ , ρ' and ρ'' resonances do not depend on the invariant mass of four pions. We use the extracted values of the mass and width of the ρ' to perform a full unbinned maximum likelihood fit of the $2\pi^-\pi^+\pi^0$ final state.

To perform this fit, we use several phenomenological models. Besides the $\omega\pi$ channel, we allow for $a_1\pi$, $\sigma\rho$, $f_0\rho$, non-resonant $\rho\pi\pi$ and non-resonant $3\pi\pi^0$ channels, as well as for their various combinations, and fit for their relative contributions to the $3\pi\pi^0$ resonant structure. This analysis shows clear dominance of the $\omega\pi$ and $a_1\pi$ components.

With a better knowledge of the four pion subchannel structure, we then perform a fit to the $\tau \rightarrow \omega\pi\nu_\tau$ spectral function assuming a mass-dependent width for the three ρ resonances.

We do not use particle identification to separate pions from kaons. A small component containing kaons (e.g., $K3\pi$) is included in the τ background, but its contribution is negligible. Generalization to charge conjugated reactions and final states is implied throughout this paper.

II. EXPERIMENT AND DATA SELECTION

We use data from the reaction $e^+e^- \rightarrow \tau^+\tau^-$ collected by the CLEO II experiment at the Cornell Electron Storage Ring (CESR) at or near the energy of the $\Upsilon(4S)$. The data correspond to a total integrated luminosity of 4.68 fb^{-1} and contain about 4.27 million $\tau^+\tau^-$ pairs.

CLEO II is a general-purpose solenoidal magnet detector [12]. The momenta of the charged particles are measured by a 67-layer drift chamber tracking system operating inside a 1.5 T superconducting solenoid. Photons and electrons are detected in a 7800-crystal

CsI electromagnetic calorimeter. Muons are identified using proportional counters placed at various depths in the return iron of the magnet yoke.

The event selection is designed to use the kinematical properties and the low multiplicity of τ decays to separate them from events copiously produced in two-photon interactions, the process $e^+e^- \rightarrow q\bar{q}$, Bhabha scattering, and muon-pair production. We select events with four charged tracks in a 1-vs-3 topology by requiring that one of the tracks must be at least 90° away from all the others. When there is more than one combination satisfying these criteria, we minimize the acolinearity angle between the momentum of the single track and the total momentum of the 3-prong system to select the most back-to-back combination. The single track hemisphere is then used as a tag associated with a one-prong τ decay to $e\bar{\nu}_e\nu_\tau$, $\mu\bar{\nu}_\mu\nu_\tau$, $\pi\nu_\tau$ or $\rho\nu_\tau$. The other three tracks and at least two well identified photons, separated by more than 90° from the tag track, are used to reconstruct the hadronic part of the signal decay $\tau \rightarrow 3\pi\pi^0\nu_\tau \rightarrow 3\pi\gamma\gamma\nu_\tau$.

To ensure well modeled acceptance, momenta of the tracks from signal and tag hemispheres must exceed $0.025E_{bm}$ and $0.05E_{bm}$ respectively, where E_{bm} is the energy of the colliding electron or positron beam and typically lies between 5.26 and 5.29 GeV. To suppress decay channels with $K_s^0 \rightarrow \pi^+\pi^-$ decays, we require that the impact parameter of charged tracks with respect to the beam axis must be less than 5 mm. The momentum of a π^0 candidate is reconstructed from the energies and directions of two photons, constrained to the mass of the π^0 . The two photon candidates must produce showers in the barrel part of the crystal calorimeter (i.e., $|\cos\theta_\gamma| < 0.71$, where θ_γ is an angle between the photon and e^+e^- beam axis) and be separated by more than 20° from the closest charged track. Energy deposition in the calorimeter is required to have a photon-like lateral profile and be greater than 75 MeV for the photon with the smaller energy and greater than 120 MeV for the photon with the higher energy. We consider only those two-photon combinations that are within 2.5 standard deviations from the nominal π^0 mass. To increase statistics for the rho tag, we also use showers in the tag hemisphere, detected both in the barrel and endcaps, with energy deposition greater than 30 MeV.

For electron identification, we require that the momentum of the track be greater than 0.5 GeV/c and that the energy deposited in the calorimeter be consistent with the momentum of the electron candidate measured by the drift chamber: $|(E/p - 1.0)| < 0.1$. We also require that the rate of energy loss due to ionization in the drift chamber must be greater than the expected rate minus two standard deviations. A track is identified as a muon if it has correlated drift and muon chamber hits and traverses at least three absorption lengths of the material, when the momentum of the track is below 2 GeV/c, and at least five absorption lengths, when the momentum of the track is above 2 GeV/c. To minimize the probability of pion-lepton misidentification for both electron and muon tags, we do not allow additional showers in the calorimeter with energy deposition greater than 120 MeV that are unmatched to any of the charged tracks. A tag track is identified as a pion if it was not identified as a lepton and if the invariant mass of the tag hemisphere is less than $0.5 \text{ GeV}/c^2$, where the invariant mass of the tag hemisphere is defined as the invariant mass of the tag track, assuming the pion mass, and all neutral showers in the tag hemisphere. A tag track is identified as a rho if it was not identified as a lepton, if the invariant mass of the two most energetic showers in the tag hemisphere is consistent with the π^0 mass within 2.5 standard deviations and, finally, if the effective mass of the tag track, assuming the pion mass, and

of the π^0 candidate lies between 0.5 and 1.2 GeV/c². To reduce combinatorial and hadronic background for the rho tag, we do not allow any showers with energy deposition greater than 120 (350) MeV in the tag hemisphere if the center of the shower is more (less) than 30 cm from the tag track projection onto the calorimeter.

A typical event, in which the decay $\tau \rightarrow 3\pi\pi^0\nu_\tau$ is tagged by a one-prong τ decay, does not deposit any significant extra energy in the calorimeter, other than that associated with either the $\pi^0 \rightarrow \gamma\gamma$ decay or with interactions between charged hadrons and CsI crystals. In most cases, additional unmatched energy deposited in the calorimeter is a signature of various background events having one or more additional π^0 's. To suppress these backgrounds, we use the value of the unmatched energy to veto such events. We reject events if there is at least one unmatched energy cluster in the calorimeter, which is not used for π^0 reconstruction, which is more (less) than 30 cm away from the closest projection of the charged track onto the calorimeter and has energy deposition more than 75 (350) MeV.

Further background reduction is based on the fact that, in a τ decay, there is always at least one neutrino carrying away undetected energy and momentum. Thus, a typical τ event has a large missing transverse momentum, P_t , whereas a typical two photon event has a small missing transverse momentum and small visible energy, E_{tot} . The transverse momentum and visible energy are measured using the four reconstructed charged tracks, assuming the pion masses for the three charged tracks in the signal hemisphere, and one π^0 (two π^0 's for the rho tag). To remove two-photon background, we use the following selection criteria [13]: $P_t > 0.1(2E_{bm} - E_{tot})$, $P_t > 0.075E_{bm}$ and $E_{tot} > 0.6E_{bm}$. To reduce background produced by Dalitz decays $\pi^0 \rightarrow e^+e^-\gamma$ or by γ conversions in the detector, we reject any event that has a well identified electron among the three charged tracks in the signal hemisphere. To reduce combinatorial $q\bar{q}$ background, we impose a requirement on the undetected neutrino mass. The neutrino mass can be calculated as:

$$M_\nu^2 = (P_\tau - P_q)^2 = M_\tau^2 + q^2 + 2|\vec{P}_\tau||\vec{P}_q| \cos \theta_{\tau q} - 2E_{bm}E_q . \quad (1)$$

Because we cannot measure $\cos \theta_{\tau q}$, we assume it to be 1 and require that the resulting maximum value of the square of the undetected neutrino mass be positive: $M_{\nu,max}^2 > 0$. In Eqn. (1) the value of M_τ is taken as 1.777 GeV/c², the momentum of the τ is expressed as $|\vec{P}_\tau| = \sqrt{E_{bm}^2 - M_\tau^2}$, the symbols q and E_q represent the invariant mass and energy of the four pion final state, and the energy of the τ is set equal to the beam energy E_{bm} .

The distribution of the $3\pi\pi^0$ effective mass, before the cut on the τ neutrino mass is applied, is plotted in Fig. 1. In the vicinity of the τ mass the production of $3\pi\pi^0$ events is strongly suppressed by phase space and the signal-to-background ratio becomes small. Hence, we accept only those events that have the effective mass of the $3\pi\pi^0$ final state lying in the range from 0.9 to 1.7 GeV/c².

After all signal selection criteria are applied, we find 25,374 data events with an estimated background of 577 ± 17 events coming from $e^+e^- \rightarrow q\bar{q}$ production and 669 ± 13 events from other τ decays. The background estimates are based on Monte Carlo. The latter background source includes contributions from $\tau^- \rightarrow 2\pi^-\pi^+2\pi^0\nu_\tau$ and $\tau^- \rightarrow \pi^-\pi^0K_s\nu_\tau \rightarrow 2\pi^-\pi^+\pi^0\nu_\tau$ decays whose yields are estimated as 1.6% and 0.7%, respectively. The τ background also includes small $K\pi\pi\pi^0$ and $KK\pi\pi^0$ components. Their contributions, calculated using the values [15] of $\mathcal{B}(\tau^- \rightarrow K^-\pi^+\pi^-\pi^0\nu_\tau) = (0.08 \pm 0.04)\%$ and $\mathcal{B}(\tau^- \rightarrow K^-K^+\pi^-\pi^0\nu_\tau) =$

$(0.069 \pm 0.030)\%$ for the branching fractions, are found to be negligible, as well as background contamination from other τ decays. The combined efficiency for all tags is estimated to be 6.75%. The measured branching fraction is $\mathcal{B}(\tau \rightarrow 3\pi\pi^0\nu_\tau) = (4.19 \pm 0.10)\%$, which does not include a conservatively estimated 5% systematic error associated with the data analysis. This is in good agreement with the Particle Data Group [15] value of $(4.35 \pm 0.10)\%$. Contamination due to 2γ physics is estimated to be completely negligible.

III. THE SPECTRAL FUNCTIONS IN $\tau \rightarrow 3\pi\pi^0\nu_\tau$ AND $\tau \rightarrow \omega\pi\nu_\tau$ DECAYS

The shape of the $3\pi\pi^0$ effective mass in τ decays is distorted by phase space and helicity factors. It is useful to examine the spectral function independent of such effects specific to τ decays.

The spectral function for $\tau \rightarrow 3\pi\pi^0\nu_\tau$ is defined [16] as:

$$V^{3\pi\pi^0}(q) = \frac{d\Gamma_{4\pi\nu}(q)}{dq} \frac{16\pi^2 M_\tau^3}{G_F^2 V_{ud}^2} \frac{1}{q(M_\tau^2 - q^2)^2(M_\tau^2 + 2q^2)}, \quad (2)$$

where $q = M(3\pi\pi^0)$, V_{ud} is an element of the CKM matrix, $M_\tau = 1.777 \text{ GeV}/c^2$ and G_F is the Fermi constant. The differential partial width can be represented as:

$$\frac{d\Gamma_{4\pi\nu}(q)}{dq} = \frac{1}{N} \frac{dN(q)}{dq} \frac{G_F^2 M_\tau^5}{192\pi^3} \frac{\mathcal{B}(\tau \rightarrow 3\pi\pi^0\nu_\tau)}{\mathcal{B}(\tau \rightarrow e\bar{\nu}_e\nu_\tau)}. \quad (3)$$

Thus, the spectral function is given by:

$$V^{3\pi\pi^0}(q) = \frac{1}{N} \frac{dN(q)}{dq} \frac{1}{q(M_\tau^2 - q^2)^2(M_\tau^2 + 2q^2)} \frac{\mathcal{B}(\tau \rightarrow 3\pi\pi^0\nu_\tau)}{\mathcal{B}(\tau \rightarrow e\bar{\nu}_e\nu_\tau)} \frac{M_\tau^8}{12\pi V_{ud}^2}. \quad (4)$$

To reduce uncertainty caused by the finite bin width, the factor $q(M_\tau^2 - q^2)^2(M_\tau^2 + 2q^2)$ in the denominator is averaged over the bin width.

In full analogy with $V^{3\pi\pi^0}(q)$, we can define a spectral function for the $\tau \rightarrow \omega\pi\nu_\tau$ decay. To extract the $\omega\pi$ component from the $3\pi\pi^0$ final state, we use a technique similar to the usual sideband subtraction. For each bin of $q = M(3\pi\pi^0)$, we select events in the ω signal region ($0.76 \text{ GeV}/c^2 < M(\pi^-\pi^+\pi^0) < 0.81 \text{ GeV}/c^2$) and fit the combined sidebands ($0.83 \text{ GeV}/c^2 < M(\pi^-\pi^+\pi^0) < 0.90 \text{ GeV}/c^2$) and ($0.60 \text{ GeV}/c^2 < M(\pi^-\pi^+\pi^0) < 0.74 \text{ GeV}/c^2$) to a second order polynomial. The fit parameters are then used to estimate the background under the ω peak. To estimate the statistical uncertainty of the non- ω component in the signal region, we propagate errors using a full covariance matrix. In addition to the statistical error for each bin, there is an uncertainty due the sideband definition. To estimate the size of this error for each bin, we vary the sideband definition and change the order of the polynomial from 2 to 1.

In Fig. 2 the shape of the $M(\omega\pi)$ distribution, which includes both ω signal and combinatorial background, is shown with solid squares. The non- $\omega\pi$ contribution is shown with dashed and dotted lines for different sideband definitions, and its average value is shown with open squares. For every bin, the error is calculated as a sum in quadrature of both statistical and systematic uncertainties.

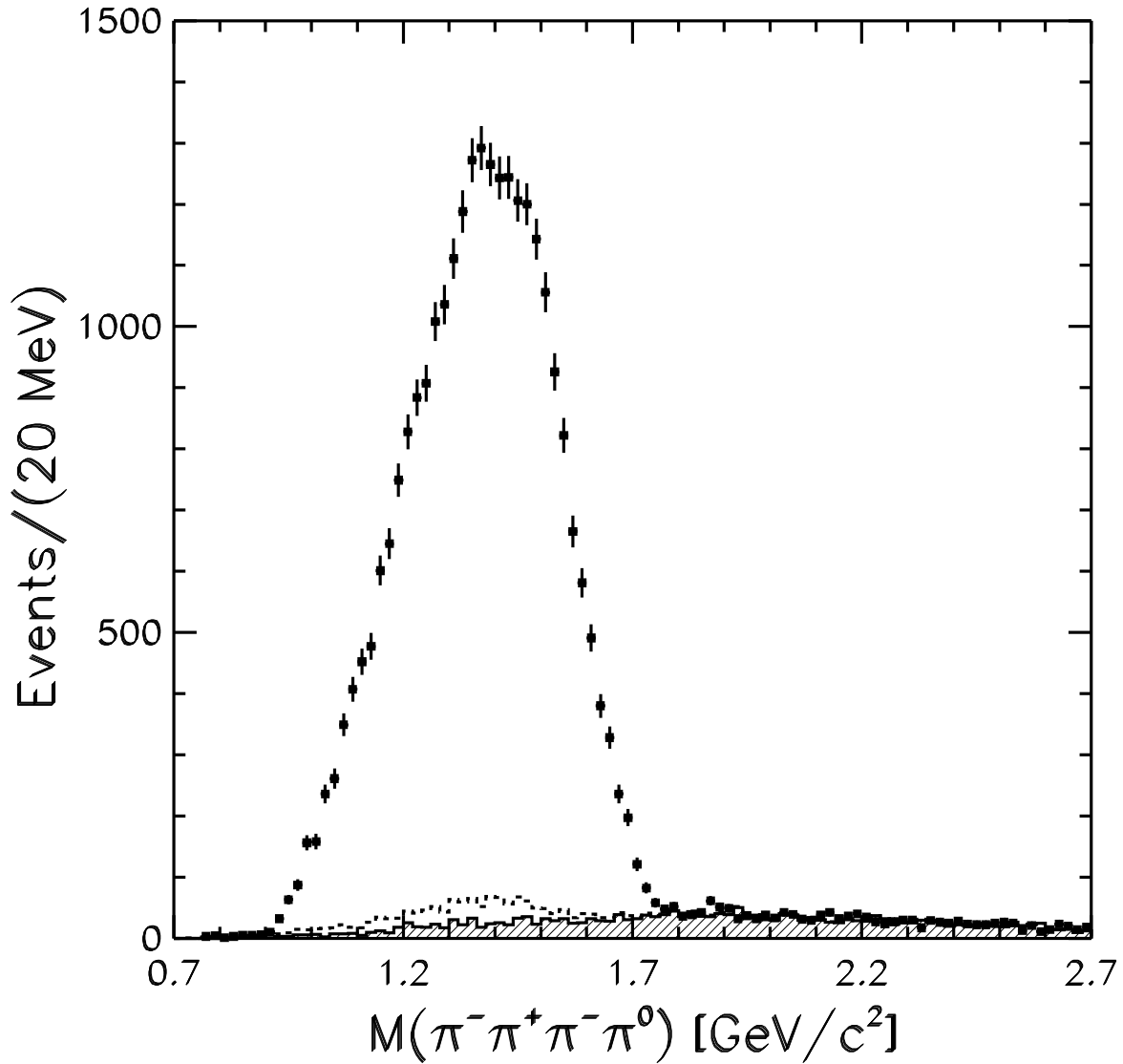


FIG. 1. The distribution of the invariant mass of $3\pi^0$ is plotted for the data (crosses), total background (dashed line) and $q\bar{q}$ background (hatched area), before the cut on the τ neutrino mass. Further analysis is limited to events between 0.9 and 1.7 GeV/c^2 .

Beginning with the distributions shown in Figs. 1 and 2, we subtract backgrounds, and apply efficiency corrections that were determined using a detailed Monte Carlo simulation of the τ decay process and the detector response. We then employ Eqn. (4) to extract the spectral functions $V^{3\pi\pi^0}(q)$ and $V^{\omega\pi}(q)$, as well as the non- $\omega\pi$ contribution $V^{non-\omega\pi}(q) \equiv V^{3\pi\pi^0}(q) - V^{\omega\pi}(q)$. All three spectral functions are shown in Fig. 3.

IV. MODEL FITS TO THE $\tau \rightarrow \omega\pi\nu_\tau$ SPECTRAL FUNCTION

The spectral function of the $\omega\pi$ component can be expressed [16] in terms of the weak form factor $F(q^2)$ as:

$$V^{\omega\pi}(q) = \frac{1}{12\pi} \left(\frac{P_\omega(q)}{q} \right)^3 \left| \frac{g_{\rho\omega\pi}}{\gamma_\rho} F(q) \right|^2. \quad (5)$$

Here, $g_{\rho\omega\pi}$ is the $\rho \rightarrow \omega\pi$ strong decay coupling, γ_ρ is a measure of the weak coupling of the ρ resonance to the weak charged current, and

$$P_\omega(q) = \sqrt{\frac{(q^2 - (M_\omega - M_\pi)^2)(q^2 - (M_\omega + M_\pi)^2)}{4q^2}} \quad (6)$$

is the momentum of the ω in the $\omega\pi$ rest frame.

The choice of the form factor $F(q)$ is largely uncertain. In the region of $q^2 \lesssim M_\tau^2$ the form factor $F(q)$ is expected to be dominated by low energy resonances. In this analysis we use a form for $F(q)$ that allows contributions from the ρ resonance and its two radial excitations ρ' and ρ'' :

$$F(q^2) = BW_\rho(q^2) + A_1 \cdot BW_{\rho'}(q^2) + A_2 \cdot BW_{\rho''}(q^2). \quad (7)$$

Here,

$$BW_\rho(q^2) = \frac{M_\rho^2}{M_\rho^2 - q^2 - iq\Gamma_\rho} \quad (8)$$

is a relativistic Breit-Wigner amplitude normalized to unity at $q^2 = 0$, and

$$A_i = \frac{g_{\rho_i\omega\pi}}{g_{\rho\omega\pi}} \frac{\gamma_\rho}{\gamma_{\rho_i}} \quad (9)$$

are the ratios of the coupling constants for the different ρ resonances.

To model the Breit-Wigner shapes (8), we first approximate Γ_ρ , $\Gamma_{\rho'}$ and $\Gamma_{\rho''}$ by constants and do not include any momentum dependence. The parameters of the $\rho(770)$ resonance have been thoroughly studied and are known with great precision [15]. In contrast, the parameters of the higher radial excitations ρ' and ρ'' are poorly known and can be used as fit variables. Unfortunately, events above 1.6 GeV/ c^2 are suppressed by phase space and provide little sensitivity for the heavy ρ'' , the mass of which is expected to be around 1.7 GeV/ c^2 . In this study we only fit for the mass and width of ρ' and keep widths and masses of ρ and ρ'' fixed at their central PDG values [15]:

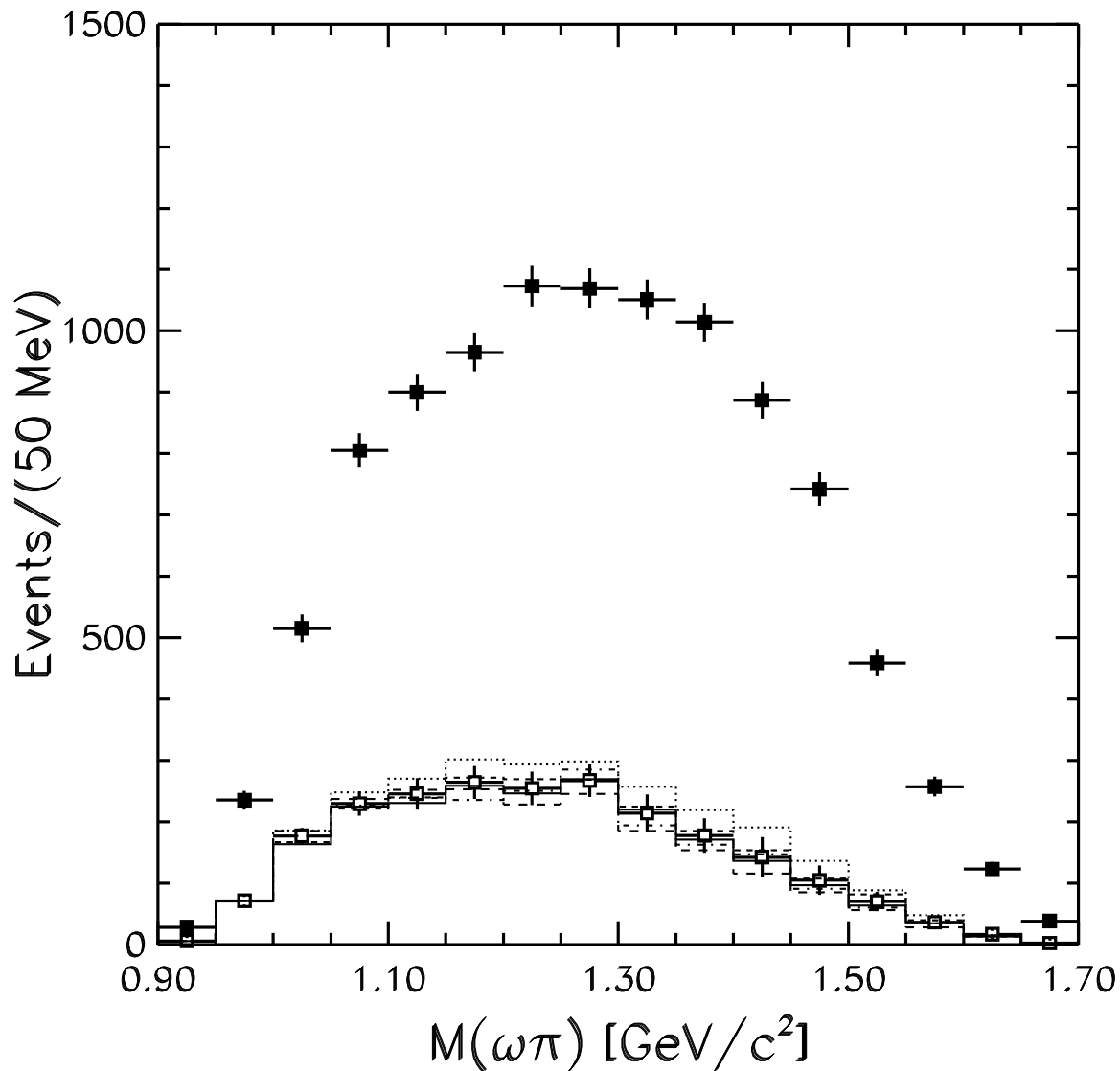


FIG. 2. Distributions of the $\omega\pi$ effective mass for events from the ω band (solid squares) and the sidebands (open squares). The ω band distribution includes combinatorial background as well. Dotted and dashed lines indicate variations in the shape of the combinatorial background due to variations in sideband definition. The estimated average background shape, with errors, is shown as open squares.

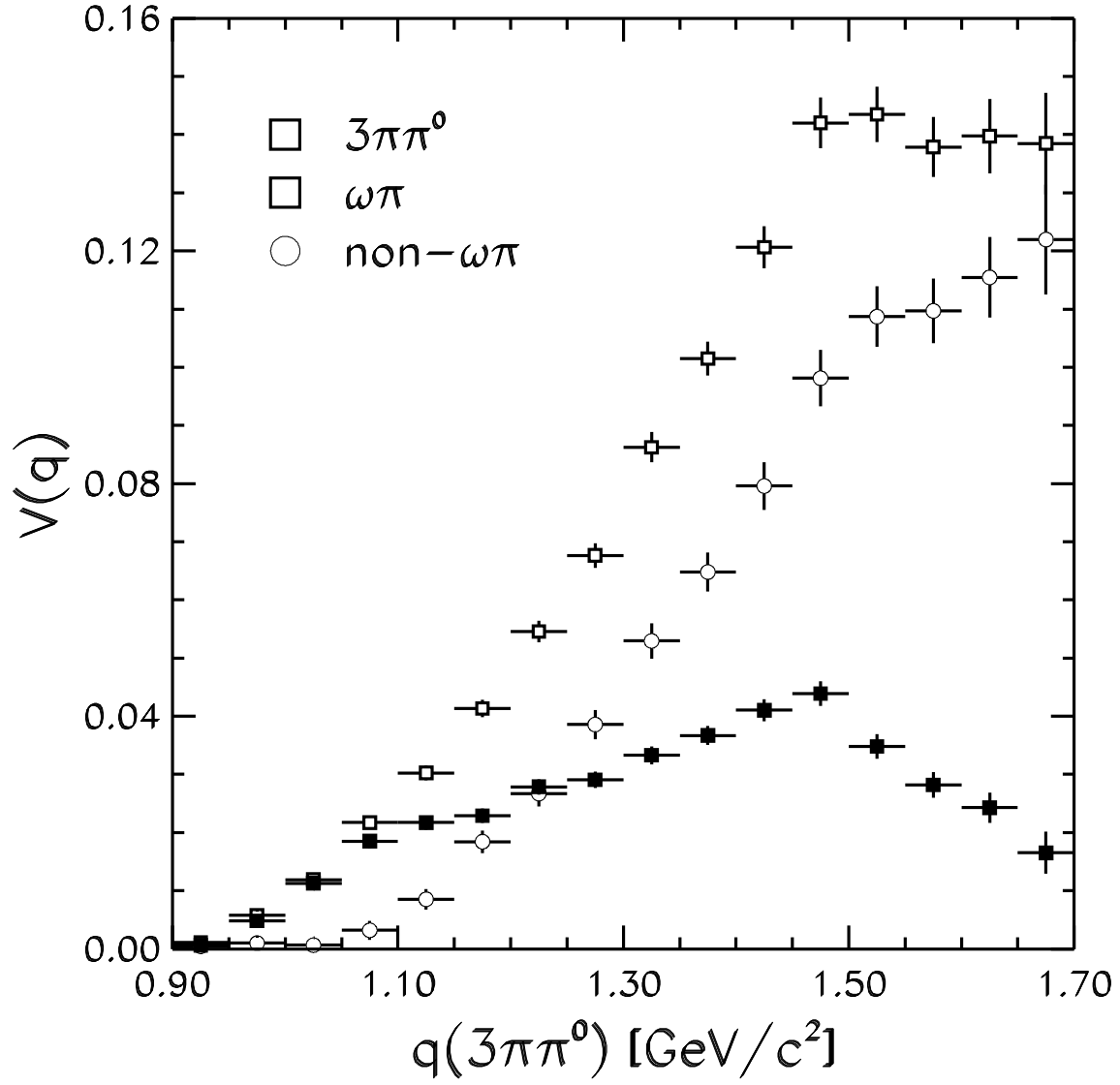


FIG. 3. Spectral functions calculated for: $3\pi\pi^0$ (open squares), $\omega\pi$ (solid squares) and non- $\omega\pi$ (open circles) components

$$M_\rho = 770 \text{ MeV}/c^2, \Gamma_\rho = 151 \text{ MeV}/c^2 ;$$

$$M_{\rho'} = 1700 \text{ MeV}/c^2, \Gamma_{\rho'} = 235 \text{ MeV}/c^2 .$$

The Conserved Vector Current (CVC) hypothesis predicts that the weak form factor and the coupling constants are equal to the corresponding electromagnetic quantities. The weak coupling $W^\pm \rightarrow \rho^\pm \rightarrow \omega\pi^\pm$ in τ decays is expected to be the same as the electromagnetic coupling $\gamma^* \rightarrow \omega\pi^0$ in the reactions $e^+e^- \rightarrow \gamma^*(q_\gamma = \sqrt{s}) \rightarrow \omega\pi^0$ and $\omega \rightarrow \gamma(q_\gamma = 0)\pi^0$. All these couplings can be presented as $g_{\rho\omega\pi}/\gamma_\rho$, where

$$\gamma_\rho = \sqrt{\frac{4\pi\alpha^2 M_\rho}{3\Gamma(\rho \rightarrow e^+e^-)}} . \quad (10)$$

Thus, one can use the Vector Dominance Model [18] to cross-check the values of A_1 and A_2 . In the VDM, the coupling constants are energy independent, and therefore the set of fitted coupling constants should reproduce the experimentally measured value of:

$$\Gamma(\omega \rightarrow \pi^0\gamma) = \frac{1}{3}\alpha P_\gamma^3 \cdot \left| \frac{g_{\rho\omega\pi}}{\gamma_\rho} [1 + A_1 + A_2] \right|^2 = (0.72 \pm 0.04) \text{ MeV}/c^2, \quad (11)$$

where P_γ is the photon momentum in the ω center-of-mass system.

To fit the data, we use the following spectral models:

- Model 1: $F(q^2) \propto |BW_{\rho(770)} + A_1 BW_{\rho'} + A_2 BW_{\rho(1700)}|^2$.
- Model 2: $F(q^2) \propto |BW_{\rho(770)} + A_1 BW_{\rho'}|^2$.
- Model 3: $F(q^2) \propto |BW_{\rho(770)} + A_2 BW_{\rho(1700)}|^2$.
- Model 4: $F(q^2) \propto |BW_{\rho(770)}|^2$.

The amplitudes A_1 and A_2 are assumed to be real. We use χ^2 minimization to fit various resonant models to the $\omega\pi$ spectral function shown in Fig. 4. To obtain the $\omega\pi$ spectral function shown in Fig. 4, we divide the $\omega\pi$ spectral function shown in Fig. 3 by a value of the branching fraction $\mathcal{B}(\omega \rightarrow \pi^+\pi^-\pi^0) = 0.888$ since the four pion final state does not include contributions from any other decays of the ω . We verified that the fit results are independent of the chosen initial values by repeating the minimization procedure with different sets of initial values.

The following parameters of the ρ' are obtained from fits to the data with Models 1 and 2:

$$\text{Model 1: } M_{\rho'} = (1.52 \pm 0.01) \text{ GeV}/c^2, \Gamma_{\rho'} = (0.38 \pm 0.04) \text{ GeV}/c^2,$$

$$\text{Model 2: } M_{\rho'} = (1.53 \pm 0.01) \text{ GeV}/c^2, \Gamma_{\rho'} = (0.43 \pm 0.03) \text{ GeV}/c^2.$$

Using these results, we calculate weighted averages of the ρ' parameters: $M_{\rho'} = (1.523 \pm 0.010) \text{ GeV}/c^2$, $\Gamma_{\rho'} = (0.400 \pm 0.035) \text{ GeV}/c^2$.

Models 3 and 4 do not provide an acceptable description of the data. Fits to our data corresponding to various combinations of the ρ resonances are displayed in Fig. 4, and the results are summarized in Table I. We conclude that the presence of a ρ' contribution is necessary to achieve an acceptable description of the data. Model 2 is favored, but Model 1 cannot be excluded.

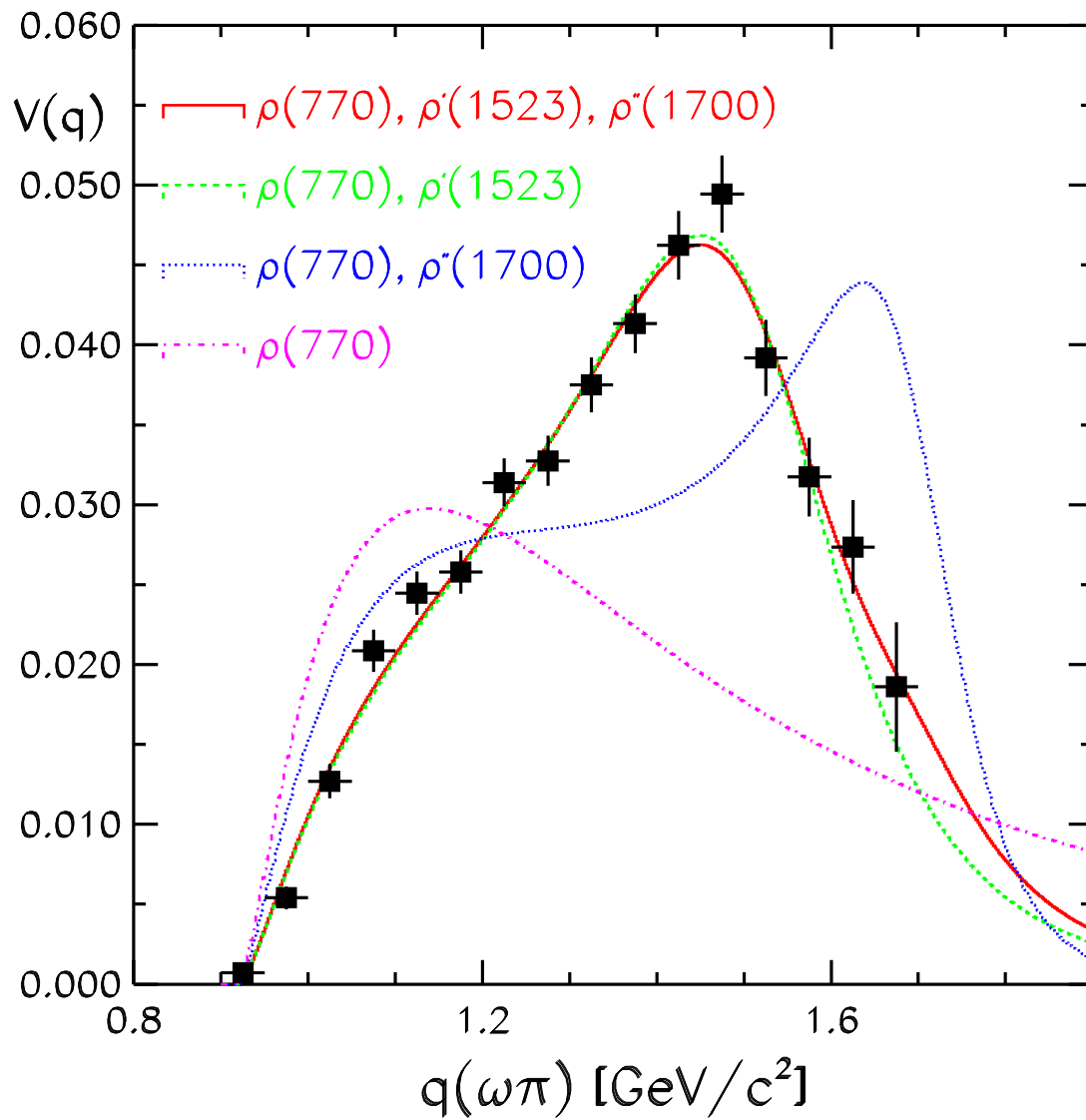


FIG. 4. Fits of the $\omega\pi$ spectral functions with various models.

TABLE I.

Fit results for various combinations of the ρ, ρ', ρ'' resonances to the $\tau \rightarrow \omega\pi\nu_\tau$ spectral function. Errors are statistical only and are strongly correlated. Errors on the total width $\Gamma(\omega \rightarrow \pi^0\gamma)$ are obtained by propagating the entire covariance matrix.

Model #	$g_{\rho\omega\pi}$ (MeV ² /c) ^{-1/2}	A ₁	A ₂	$\chi^2/d.o.f.$	$\Gamma(\omega \rightarrow \pi^0\gamma)$ MeV
1	16.4 ± 0.6	-0.20 ± 0.04	-0.017 ± 0.016	16.1/11	0.87 ± 0.15
2	16.1 ± 0.6	-0.24 ± 0.02		16.6/12	0.78 ± 0.10
3	22.7 ± 0.2		-0.067 ± 0.017	342/14	2.3 ± 0.05
4	27.2 ± 0.2			940/15	3.9 ± 0.03
$\Gamma(\omega)\mathcal{B}(\omega \rightarrow \pi^0\gamma)$					0.72 ± 0.04

V. INCLUSION OF MASS-DEPENDENT WIDTHS INTO THE FIT OF THE $\tau \rightarrow \omega\pi\nu_\tau$ SPECTRAL FUNCTION

We now perform a fit to the $\tau \rightarrow \omega\pi\nu_\tau$ spectrum assuming a mass-dependent width for the three ρ resonances. For this purpose, we use the results of Section VII E. We choose the model that includes contributions from $\omega\pi$, $\rho\pi\pi$, and non-resonant $3\pi\pi^0$ channels and use the extracted values of $R_{\rho^0\pi^-\pi^0}$, $R_{\rho^-\pi^-\pi^+}$, $R_{\rho^+\pi^-\pi^-}$ and $R_{\omega\pi}$ to perform a numerical integration in momentum space in order to obtain a spectral decomposition of the $\tau \rightarrow 3\pi\pi^0\nu_\tau$ channel. The results of the integration are shown in Table II. Here and below, we use the value of the mass of the ρ' extracted from the fits to the $\omega\pi$ spectral function as described in the previous Section.

TABLE II.

Contributions to the spectral functions of the $\omega\pi$ and $\rho\pi\pi$ subchannels of $\tau \rightarrow 3\pi\pi^0\nu_\tau$.

	$\omega\pi$	$\rho\pi\pi$
non-resonant	7%	76%
$\rho(770)$	36%	0.2%
$\rho'(1520)$	12%	5%
constructive interference	47%	20%

With a better understanding of the $\omega\pi$ and $\rho\pi\pi$ spectral functions, we perform a fit to the $\tau \rightarrow \omega\pi\nu_\tau$ spectrum assuming mass-dependent widths for the three ρ resonances. Instead of constant-width Breit-Wigner shapes (8), we use mass-dependent total widths $\Gamma_i(q^2)$; $i = \rho, \rho', \rho''$. To simulate the mass-dependent widths, we follow the approach adopted in Ref. [6].

Since $\rho \rightarrow \pi\pi$ is the dominant ρ decay mode, we take into account only this channel for the calculation of $\Gamma_\rho(q^2)$:

$$\Gamma_\rho(q^2) = \Gamma_{\rho 0} \frac{M_\rho}{q} \left(\frac{p_\pi(q^2)}{p_\pi(M_\rho^2)} \right)^3, \quad (12)$$

where $\Gamma_{\rho 0} = 151$ MeV and $M_\rho = 770$ MeV are the central width and mass of the ρ resonance fixed at their PDG values [15], q is the hadronic four-momentum, $p_\pi(q^2) = \sqrt{q^2/4 - M_\pi^2}$ is the pion momentum in the ρ rest frame, and $p_\pi(M_\rho^2)$ is the same momentum evaluated at the pole mass of the ρ resonance.

For the total width of the ρ' resonance, we take into account only contributions from $\rho' \rightarrow \pi\pi$, $\rho' \rightarrow \omega\pi$ and $\rho' \rightarrow \rho\pi\pi$ modes:

$$\Gamma_{\rho'}(q^2) = \Gamma_{\rho' 0} \left[\mathcal{B}(\rho' \rightarrow \pi\pi) \frac{M_{\rho'}}{q} \left(\frac{p_\pi(q^2)}{p_\pi(M_{\rho'}^2)} \right)^3 + \mathcal{B}(\rho' \rightarrow \omega\pi) \frac{M_{\rho'}}{q} \left(\frac{p_\omega(q^2)}{p_\omega(M_{\rho'}^2)} \right)^3 + \mathcal{B}(\rho' \rightarrow \rho\pi\pi) \frac{F_{\rho\pi\pi}(q^2)}{F_{\rho\pi\pi}(M_{\rho'}^2)} \right], \quad (13)$$

where $\Gamma_{\rho' 0}$ and $M_{\rho'}$ are the central width and mass of the ρ' resonance that are allowed to float in the fit, $\mathcal{B}(\rho' \rightarrow \pi\pi)$, $\mathcal{B}(\rho' \rightarrow \omega\pi)$ and $\mathcal{B}(\rho' \rightarrow \rho\pi\pi)$ are relative branching fractions normalized with their sum is equal to one, and $p_\omega(q^2)$ is the momentum of the ω in the $\omega\pi$ rest frame (6). To extract the shape of $F_{\rho\pi\pi}(q^2)$, we generate a $\tau \rightarrow \rho\pi\pi\nu_\tau$ sample with overall phase-space and $\omega\pi$ contributions eliminated. The form factor is defined as:

$$F_{\rho\pi\pi}(q^2) = \frac{1}{(M_\tau^2 + 2q^2)(M_\tau^2 - q^2)^2} \frac{1}{q} \frac{dN}{dq}, \quad (14)$$

where dN/dq is the number of Monte-Carlo events in a given bin of the invariant mass q . To obtain the shape parameters, we fit the form factor to a second order polynomial.

The choice of the relative branching fractions of ρ' is largely uncertain [15]. The ratio $\mathcal{B}(\rho' \rightarrow \rho\pi\pi)/\mathcal{B}(\rho' \rightarrow \omega\pi)$ can be extracted from our data. The relative contributions of the ρ' resonance into the $\omega\pi$ and $\rho\pi\pi$ spectral functions, shown in Table II, are 12% and 5% respectively. Hence, the ratio of the branching fractions is estimated as:

$$\frac{\mathcal{B}(\rho' \rightarrow \rho\pi\pi)}{\mathcal{B}(\rho' \rightarrow \omega\pi)} = \frac{0.05 \mathcal{B}(\tau \rightarrow \rho\pi\pi\nu_\tau)}{0.12 \mathcal{B}(\tau \rightarrow \omega\pi\nu_\tau)},$$

where the ratio $\mathcal{B}(\tau \rightarrow \rho\pi\pi\nu_\tau)/\mathcal{B}(\tau \rightarrow \omega\pi\nu_\tau)$ is given by the results of our multidimensional fit described in Section VII E. We obtain $\mathcal{B}(\rho' \rightarrow \rho\pi\pi)/\mathcal{B}(\rho' \rightarrow \omega\pi) = 0.61$ and vary the value of $\mathcal{B}(\rho' \rightarrow \pi\pi)$ in the fit to make sure that the outcome depends weakly on the input value. For the final result shown in Fig. 5, we use the constraint [15] $\mathcal{B}(\rho' \rightarrow \pi\pi)/\mathcal{B}(\rho' \rightarrow \omega\pi) \sim 0.32$.

To simulate the mass-dependent width of the ρ'' , we account only for the $\rho'' \rightarrow \rho\pi\pi$ decay, since PDG [15] suggests that this is the dominant mode. The mass-dependent width of the ρ'' is calculated similarly to the $\rho' \rightarrow \rho\pi\pi$ contribution:

$$\Gamma_{\rho''}(q^2) = \Gamma_{\rho'' 0} \frac{F_{\rho\pi\pi}(q^2)}{F_{\rho\pi\pi}(M_{\rho''}^2)}, \quad (15)$$

where $\Gamma_{\rho''_0} = 1700$ MeV and $M_{\rho''} = 235$ MeV are the central width and mass of the ρ'' resonance fixed at their PDG values [15], and $F_{\rho\pi\pi}(q^2)$ has the same shape as for $\Gamma_{\rho'}(q^2)$.

Assuming this model, we fit the $\tau \rightarrow \omega\pi\nu_\tau$ spectral function to the data. We make two fits: 1) the contribution of the ρ'' resonance is set to zero, and 2) the contribution of the ρ'' is allowed to float in the fit. In both situations the extracted mass of the ρ' is close to that of the ρ'' . Hence, we cannot distinguish between the two resonances, and we assume that the shape of the spectral function is affected by the ρ' resonance only. The extracted mass and width of the ρ' are 1.67 ± 0.03 GeV and 0.8 ± 0.1 GeV, respectively. The fit is shown in Fig. 5.

We also fit for the ρ' and ρ'' contributions fixing the masses and widths of ρ' and ρ'' to their PDG values. The obtained fit does not reproduce the shape of the measured spectral function, which implies that the given combination of ρ' and ρ'' parameters does not provide an adequate description of the data.

Finally, we attempt to fit for the relative phases of A_1 and A_2 , i.e., of ρ' and ρ'' contributions, respectively. Our study shows that, varying the phases within $\pm\pi/4$, we do not introduce any significant changes in the shape of the spectral function. Hence, we can argue neither in favor of non-zero phases, nor in favor of phaseless models, and we set the phases to zero for simplicity.

We also fit the $\tau \rightarrow \omega\pi\nu_\tau$ spectral function, assuming another parameterization of the total width of the ρ' resonance. Now the $\rho' \rightarrow \rho\pi\pi$ contribution is replaced by that of $\rho' \rightarrow a_1\pi$ because Section VII E suggests that the four pion spectrum is dominated by the $\omega\pi$ and $a_1\pi$ channels. The last term in Eqn. (13) is therefore replaced with $\mathcal{B}(\rho' \rightarrow a_1\pi)(M_{\rho'}/q)(p_{a_1}(q^2)/p_{a_1}(M_{\rho'}^2))$, where $\mathcal{B}(\rho' \rightarrow a_1\pi)$ is estimated using the results of Section VII E. The extracted values of the mass and width of the ρ' are similar to those quoted in this Section, i.e., significantly larger than the values obtained with the mass-independent fit.

Because fits assuming mass-dependent widths rely heavily on the choice of the model for the width parameterization, we use the mass and width of ρ' obtained in the fits with the mass-independent width (Section IV). The analysis described in this Section is presented mostly as a cross-check.

VI. SEARCH FOR SECOND CLASS CURRENTS IN $\tau \rightarrow \omega\pi\nu_\tau$ DECAY

The decay $\tau \rightarrow \omega\pi\nu_\tau$ is expected to proceed through the hadronic vector current mediated by ρ , ρ' , ρ'' and higher excitations. If, however, G parity conservation is broken due to second class currents [17], the decay can proceed through a hadronic axial-vector current mediated, e.g., by the $b_1(1235)$ resonance. The difference in spin-parity assignments for each of these states is reflected in different polarizations of the ω spin and hence in different expected angular distributions of $\cos\chi$. The angle χ is defined as the angle between the normal to the ω decay plane and the direction of the fourth pion measured in the ω rest frame, and L is the orbital angular momentum of the $\omega\pi$ system. The expected forms [19] of the $\cos\chi$ distribution are listed in Table III.

We form the distribution of $\cos\chi$ for the $\tau \rightarrow \omega\pi\nu_\tau$ events in our data. To eliminate combinatorial and non- ω background, we perform a sideband subtraction for every bin, in

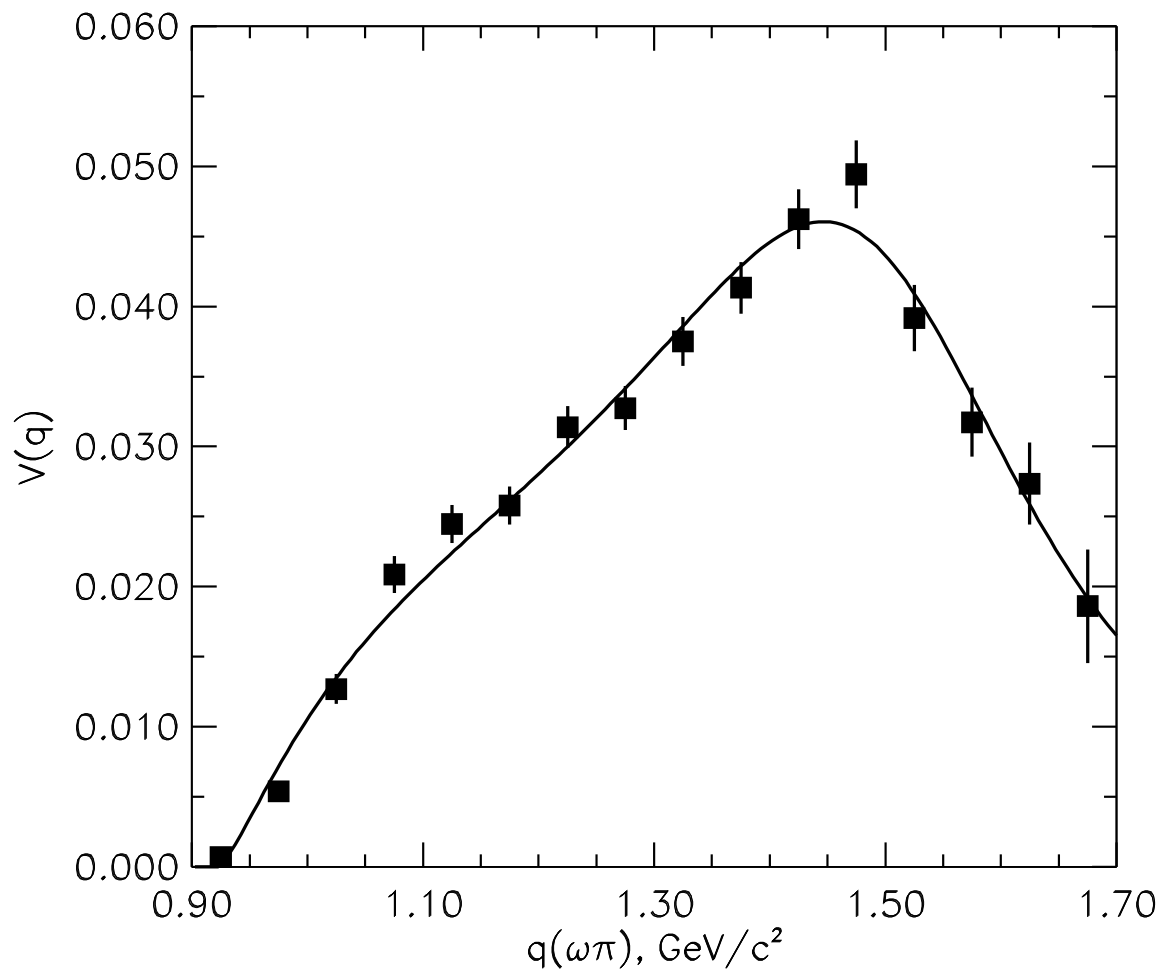


FIG. 5. Fit of the $\omega\pi$ spectral function with mass-dependent width.

TABLE III.

Expected shapes for different spin-parity assignments in the decay $\tau \rightarrow \omega\pi\nu_\tau$.

J^P	L	$F(\cos\chi)$
1^-	1	$1 - \cos^2\chi$
1^+	0	1
1^+	2	$1 + 3\cos^2\chi$
0^-	1	$\cos^2\chi$

the same way as described in Section III. Using Monte Carlo estimates, we subtract small ω contributions from τ and $q\bar{q}$ background events, correct for efficiency, and fit the resulting distribution, shown in Fig. 6, with the following function:

$$F = (1 - \epsilon) \cdot F^1 + \epsilon \cdot F^2 . \quad (16)$$

Here, $F^1(\cos\chi) = 1 - \cos^2\chi$ is the shape of the dominant vector contribution and $F^2(\cos\chi) = 1$ represents the shape which gives the most conservative estimate of the non-standard contribution to the $\tau \rightarrow \omega\pi\nu_\tau$ decay. The value of ϵ obtained from the fit is consistent with zero within errors: $\epsilon = (0.08 \pm 2.00) \times 10^{-2}$. After integration, it can be translated into an upper limit on the ratio $N^{\omega\pi}(\text{non-vector current})/N^{\omega\pi}(\text{vector current}) < 5.4\%$ at 90% CL and $< 6.4\%$ at 95% CL, where $N^{\omega\pi}$ represents the number of events generated through the corresponding current. An analogous study [4] by ALEPH yielded $N^{\omega\pi}(\text{non-vector current})/N^{\omega\pi}(\text{vector current}) < 8.6\%$ at 95% CL. The solid line in Fig. 6 illustrates the agreement of the $(1 - \cos^2\chi)$ description and the data.

VII. FULL UNBINNED LIKELIHOOD FIT TO THE $\tau \rightarrow 3\pi\pi^0\nu_\tau$ RESONANT STRUCTURE

A general method of obtaining a resonant decomposition of a hadronic final state is a partial wave analysis of the data via an unbinned maximum likelihood fit. For any data set with limited statistics, the analysis is model-dependent since there is a necessary choice of amplitudes to be considered. In this study, we consider four models with contributions from $\omega\pi$, $a_1\pi$, $\sigma\rho$, $f_0\rho$, $\rho\pi\pi$, and non-resonant $3\pi\pi^0$ channels.

Results depend on the model chosen for the hadronic current parameterization. A general description and some details of the formalism are given below. The amplitude description is given in the Appendix.

A. Definition of the fit function

The differential width of the τ decay into the $3\pi\pi^0$ final state is described by a factorizable sequence of decays: $\tau \rightarrow h + \nu_\tau$ followed by $h \rightarrow 4\pi$, and can be expressed as:

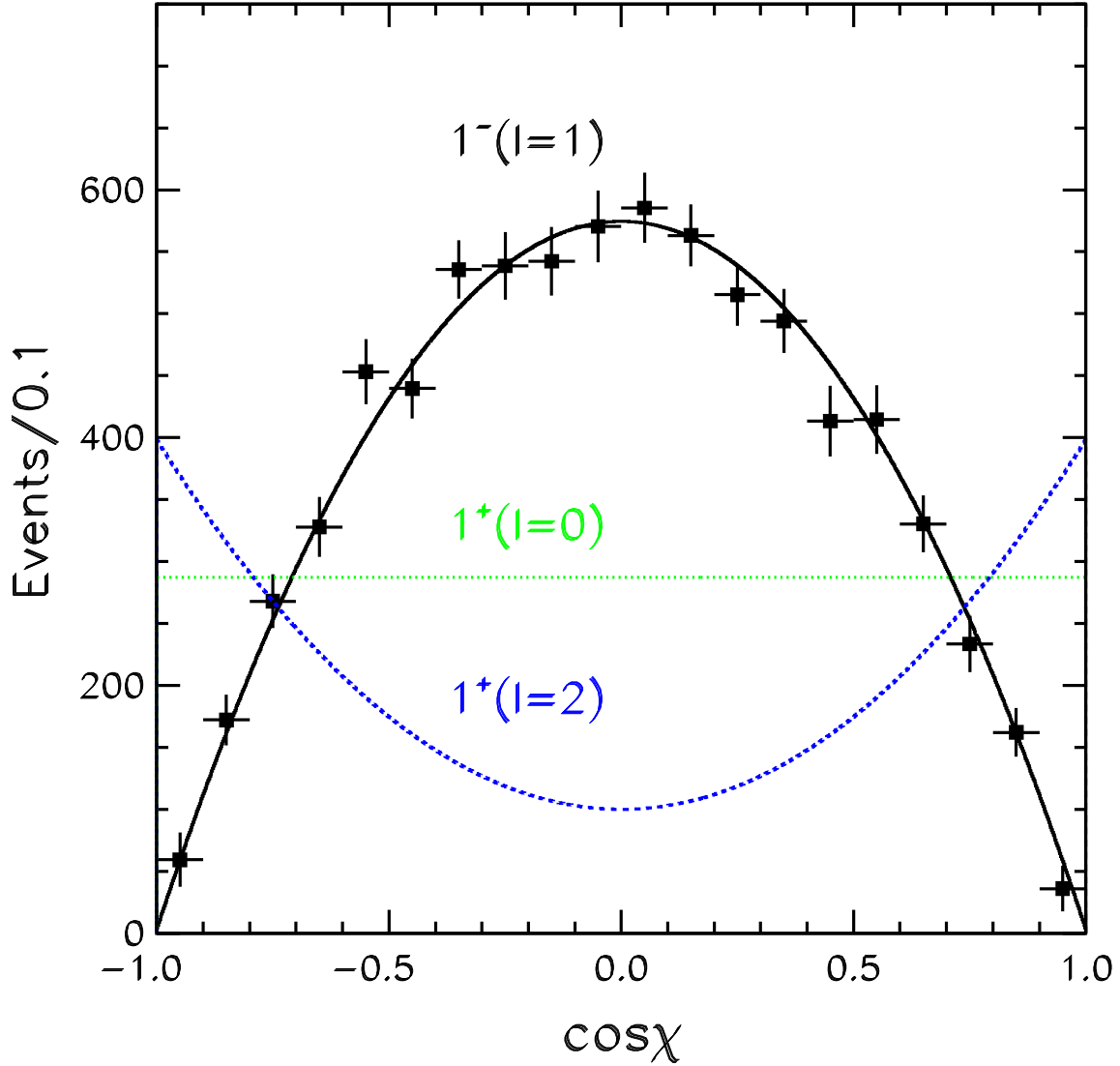


FIG. 6. The distribution of $\cos \chi$ for $\tau \rightarrow \omega\pi\nu_\tau$ events after background subtraction and efficiency correction is shown as filled squares with error bars. The solid line represents a fit to the vector current model $J_L^P = 1_1^-$, the dashed line shows the expected shape for $J_L^P = 1_2^+$, and the dotted line shows the $J_L^P = 1_0^+$ model.

$$d\Gamma(\tau \rightarrow 3\pi\pi^0\nu_\tau) = \frac{1}{2M_\tau} |\mathcal{M}|^2 d\text{LIPS}(\tau \rightarrow \nu_\tau h) d\text{LIPS}(h \rightarrow 3\pi\pi^0), \quad (17)$$

where

$$|\mathcal{M}|^2 = \frac{G_F^2}{2} V_{ud}^2 L^{\mu\nu} H_{\mu\nu} \quad (18)$$

is the square of the corresponding matrix element, $d\text{LIPS}$ is an element of the phase space volume, and $L^{\mu\nu}$ and $H_{\mu\nu}$ are lepton and hadronic tensors, respectively.

The lepton tensor $L^{\mu\nu}$ cannot be calculated without information on the neutrino direction. To resolve this problem, we use a general form of the matrix element proposed by Mirkes and Kühn [7] which is explicitly averaged over the neutrino direction. In this approach the averaged matrix element is expressed as a sum of 16 terms:

$$\overline{L^{\mu\nu} H_{\mu\nu}} = 2(M_\tau^2 - q^2) \sum_{i=1}^{16} \overline{L_i} W_i, \quad (19)$$

where the weights W_i can be calculated from components of the complex hadronic current J_μ , and $\overline{L_i}$ are kinematic parameters which depend only on the four-momenta of the four pions in the $3\pi\pi^0$ final state.

To calculate J_μ , we use the KORALB Monte Carlo program with the TAUOLA decay package [20]. The reconstructed four-momenta of the $2\pi^-\pi^+\pi^0$ system are boosted into the rest frame of the hadronic system which is denoted by the superscript “ cm ”. They are then projected onto the following coordinate system: the x -axis is along the direction of $(\vec{P}_{\pi^+}^{cm} + \vec{P}_{\pi^0}^{cm})$, the z -axis is perpendicular to the plane defined by the vectors $\vec{P}_{\pi_1^-}^{cm}$ and $\vec{P}_{\pi_2^-}^{cm}$, and the y -axis is perpendicular to the $x - z$ plane. We found that the calculated weights reveal large unphysical fluctuations unless we require $\cos\psi > -0.97$, where ψ is the angle between the direction of the laboratory and the τ , as seen from the hadronic rest frame [6].

To check whether the calculation of the $\overline{L^{\mu\nu} H_{\mu\nu}}$ expression is correct, we choose a parameterization of the hadronic current with form factors and coupling constants that provide a good description of the data. We generate a large sample of $\tau \rightarrow 3\pi\pi^0\nu_\tau$ events according to the phase space and for each event we calculate the corresponding averaged weight: $\overline{L^{\mu\nu} H_{\mu\nu}}$. As a cross check, we use the same parameterization of the hadronic current to generate another sample of unit weight events using the standard full TAUOLA simulation. The full $\tau \rightarrow 3\pi\pi^0\nu_\tau$ simulation invokes explicit generation of neutrino momenta and subsequent calculation of the precise matrix element $L^{\mu\nu} H_{\mu\nu}$. In the limit of large statistics, both methods should give the same results. The shapes of submass and total hadronic energy distributions generated with both methods agree, though the distributions obtained with the averaged matrix element reveal a higher level of fluctuations. This is due to the fact that the averaging over the neutrino direction introduces an additional smearing which increases errors.

B. Likelihood function

The matrix element averaged over the neutrino direction can be used as a probability density function (p.d.f.) to fit the data of the $\tau \rightarrow 3\pi\pi^0\nu_\tau$ decays. The fitting technique is a straightforward extension of that used to fit three-body Dalitz plots.

We take advantage of the following convenient notation [13]. The matrix element $\mathcal{M}(\vec{\alpha}, \vec{\beta}|\vec{\theta})$ is described by a model parameter vector $\vec{\theta}$ which consists of resonant amplitudes and phases. The matrix element is a function of observable variables $\vec{\alpha}$ (e.g., hadronic four-momenta) and non-observable variables $\vec{\beta}$ (e.g., neutrino four-momentum). The matrix element has to be integrated over the non-observable variables:

$$f_s(\vec{\alpha}|\vec{\theta}) = \int |\mathcal{M}(\vec{\alpha}, \vec{\beta}|\vec{\theta})|^2 d\vec{\beta}, \quad (20)$$

where $f_s(\vec{\alpha}|\vec{\theta})$ is the probability to observe a final state with a parameter vector $\vec{\alpha}$, given the model parameters $\vec{\theta}$. To compare directly with the data distribution, f_s must be multiplied by the phase space function $\phi(\vec{\alpha})$ and by the detector acceptance $\eta(\vec{\alpha})$:

$$f_s^{exp}(\vec{\alpha}|\vec{\theta}) = \eta(\vec{\alpha})\phi(\vec{\alpha})f(\vec{\alpha}|\vec{\theta}). \quad (21)$$

Since we are trying to determine parameters of the matrix element and have all observables fixed by data, we follow the usual Bayesian practice and exchange the argument and the parameter in the expression for f_s^{exp} , thus interpreting it as a probability distribution for $\vec{\theta}$, given the event observables $\vec{\alpha}$.

Since the parameters of the p.d.f are varied in the fit, the normalization of the matrix element is no longer constant and must be recalculated on each step of the fit:

$$F_s = \frac{f_s(\vec{\theta}|\vec{\alpha})}{N(\vec{\theta})} = \frac{f_s(\vec{\theta}|\vec{\alpha})}{\int \eta(\vec{\alpha})\phi(\vec{\alpha})f_s(\vec{\theta}|\vec{\alpha})d\vec{\alpha}}. \quad (22)$$

Due to the presence of background, we must also include a corresponding background p.d.f. F_b , and define the total p.d.f. as:

$$F = \frac{R_{S/B}F_s + F_b}{R_{S/B} + 1}, \quad (23)$$

where $R_{S/B}$ is a signal-to-background ratio. The likelihood function for selected events is defined as:

$$\mathcal{L}(\vec{\theta}) = \prod_{events} F^{exp} = \prod_{events} \frac{R_{S/B}F_s + F_b}{R_{S/B} + 1} \eta(\vec{\alpha})\phi(\vec{\alpha}). \quad (24)$$

To find the maximum of the likelihood, we minimize $-2Ln\mathcal{L}$, where

$$Ln\mathcal{L}(\vec{\theta}) = \sum_{j=1}^N Ln \frac{R_{S/B}F_s + F_b}{R_{S/B} + 1} + \sum_{j=1}^N Ln(\eta(\vec{\alpha})\phi(\vec{\alpha})). \quad (25)$$

The term $\sum Ln(\eta(\vec{\alpha})\phi(\vec{\alpha}))$ is constant for the purpose of minimizing F and is therefore neglected. Thus, we never need to explicitly evaluate $\eta(\vec{\alpha})$ and $\phi(\vec{\alpha})$: the amplitude normalization $N(\vec{\theta})$ obtained by Monte Carlo techniques takes them into account automatically. When parameter terms can be factored out, the computation of the normalization $N(\vec{\theta})$ can be speeded up:

$$N(\vec{\theta}) = \int \eta(\vec{\alpha})\phi(\vec{\alpha})f(\vec{\theta}|\vec{\alpha})d\vec{\alpha} = \int \eta(\vec{\alpha})\phi(\vec{\alpha}) \left[\sum_j C_j(\vec{\theta})f_j(\vec{\alpha}) \right] d\vec{\alpha} = \sum_j C_j(\vec{\theta}) \int \eta(\vec{\alpha})\phi(\vec{\alpha})f_j(\vec{\alpha})d\vec{\alpha}, \quad (26)$$

where the index j runs over all possible combinations of the fit parameters $\vec{\theta}$. During the fit, the integrals in the above expression are calculated only once and then multiplied by the coefficients C_j which depend on the parameters $\vec{\theta}$ only.

C. Signal p.d.f.

As shown in Section VII B, all constant factors and functions of observable variables $\vec{\alpha}$ that multiply the signal p.d.f. (20) do not change the position of a maximum of the likelihood function (24) in the parameter space $\vec{\theta}$. Neglecting such contributions, the signal p.d.f (20) can be expressed as:

$$f_s = \overline{L^{\mu\nu}H_{\mu\nu}} = \sum_1^{16} \overline{L_i}W_i. \quad (27)$$

The hadronic current for the decay $\tau^- \rightarrow 2\pi^-\pi^+\pi^0\nu_\tau$ is parameterized as follows:

$$J^\mu = \alpha_\omega f_\omega^\mu F_\omega(q) + \sum_k \alpha_k f_k^\mu F_k(q), \quad (28)$$

where q is the total hadronic four-momentum. The spectral functions (amplitude form factors) are defined as sums of the corresponding Breit-Wigner amplitudes

$$F_k(q) = \beta_k^0 + \beta_k BW_\rho(q) + \beta_k' BW_{\rho'}(q) + \beta_k'' BW_{\rho''}(q); \quad (29)$$

the coefficients f_k^μ are functions of four-momenta describing the shapes of the corresponding contributions, the coefficients α_k are complex amplitudes, the coefficients β_k , β_k' and β_k'' are complex amplitudes of the k th spectral function component, and the sum in Eqn. (28) is taken over all non- ω contributions, as described in Section VII E below. For practical purposes, the amplitude of one of the α_k is set to a non-zero constant and the phase of one of the α_k is set to zero; the corresponding rescaling factors are then included into the other amplitudes, while the overall normalization of the signal p.d.f. is set to unity. The explicit form of the form factor f_ω^μ is based on Refs. [14,20,23], which employs correct ω helicity factors and proper symmetrization.

From the fit, we determine the amplitudes α_k for the decay $\tau \rightarrow 2\pi^-\pi^+\pi^0\nu_\tau$. We integrate these amplitudes over a large sample of $\tau \rightarrow 3\pi\pi^0\nu_\tau$ events to translate them into relative branching fractions.

D. Background p.d.f.

The total background in the selected data sample is estimated to be 4.9%. Because it is small, we do not calculate a p.d.f. for each individual component separately. Instead, we use

a simpler, empirical approach: we reweight the $3\pi\pi^0$ phase space to create an effective matrix element describing the shape of the sum of the τ and $q\bar{q}$ backgrounds that was determined using detailed Monte Carlo simulations. We use a purely empirical form of this effective matrix element:

$$\begin{aligned}
F_b = & (M_\tau^2 - M(3\pi\pi^0)^2) \times (1 + \\
& \frac{0.8}{(M(\pi^0\pi_1^-)^2 - M_\rho^2)^2 + \Gamma_\rho^2} + \frac{0.8}{(M(\pi^0\pi_2^-)^2 - M_\rho^2)^2 + \Gamma_\rho^2} + \\
& \frac{0.011}{(M(\pi^0\pi^+\pi_1^-)^2 - M_\omega^2)^2 + \Gamma_\omega^2} + \frac{0.011}{(M(\pi^0\pi^+\pi_2^-)^2 - M_\omega^2)^2 + \Gamma_\omega^2} + \\
& \left. \frac{0.005}{(M(\pi_1^-\pi^+)^2 - M_{K_s}^2)^2 + \Gamma_{K_s}^2} + \frac{0.005}{(M(\pi_2^-\pi^+)^2 - M_{K_s}^2)^2 + \Gamma_{K_s}^2} \right). \tag{30}
\end{aligned}$$

The choice of the parameterization is largely *ad hoc*, the coefficients are tuned to describe the background distributions in seven mass projections, as shown in Fig. 7. These distributions are obtained from Monte Carlo simulations of τ backgrounds and an appropriately scaled contribution from $e^+e^- \rightarrow q\bar{q}$ continuum events.

E. Fits to various models

We use 4 models to parameterize the hadronic current. The models account for the following contributions:

- Model 1: $\omega\pi$, $\rho\pi\pi$ and non-resonant $3\pi\pi^0$;
- Model 2: $\omega\pi$ and $a_1\pi$;
- Model 3: $\omega\pi$, $a_1\pi$, $\sigma\rho$ and $f_0(980)\rho$;
- Model 4: $\omega\pi$, $a_1\pi$ and $\rho\pi\pi$.

Hadronic current expressions for each model are given in the Appendix. For the $\rho\pi\pi$ contribution, the spectral functions for the $\rho^-\pi^+\pi^-$, $\rho^0\pi^0\pi^-$ and $\rho^+\pi^-\pi^-$ components are assumed to be identical, and the corresponding form factors f_i^μ are parameterized in the same way as it is done in the TAUOLA package [20]. We use the PDG [15] value for the mass of the a_1 resonance ($M_{a_1} = 1230$ MeV) and adopt the prescription of Ref. [5] to use the higher end of the width interval recommended by PDG ($\Gamma_{a_1} = 600$ MeV). For the mass and width of σ , i.e., $f_0(400 - 1200)$ in PDG's notation, we assume values [24] of $M_\sigma = 860$ MeV and $\Gamma_\sigma = 880$ MeV. We use PDG values for the mass and width of the $f_0(980)$ of $M_{f_0} = 980$ MeV and $\Gamma_{f_0} = 70$ MeV. To obtain the relative contributions of the $\tau \rightarrow 3\pi\pi^0\nu_\tau$ decay components, the fit parameters are integrated over 300,000 of $3\pi\pi^0$ phase space events and renormalized. Fit errors are propagated in accordance with this procedure. We use the following definition: $R_i = \mathcal{B}_i/\mathcal{B}(\tau^- \rightarrow 2\pi^-\pi^+\pi^0\nu_\tau)$, where \mathcal{B}_i is a branching fraction for the corresponding channel, e.g., $R_{a_1\pi} = \mathcal{B}(\tau^- \rightarrow (a_1\pi)^-\nu_\tau)/\mathcal{B}(\tau^- \rightarrow 2\pi^-\pi^+\pi^0\nu_\tau)$. Statistical errors on the relative fractions R_i are obtained from the maximum likelihood fits assuming one standard deviation.

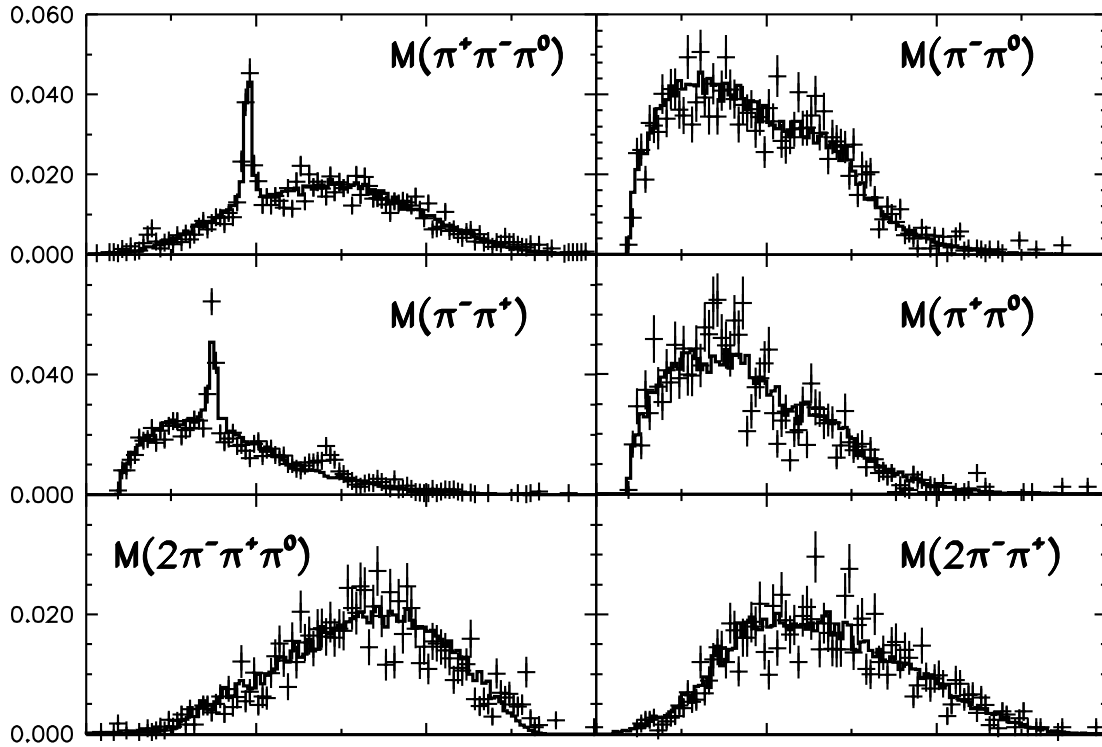


FIG. 7. Background parameterization plotted for different submass projections. The predictions from Monte Carlo simulations are shown with crosses. The background parameterization is shown as a histogram.

To simulate the form factors $BW_{\rho'}$, BW_{a_1} and BW_{σ} , we used both fits with mass-dependent and mass-independent widths. The observed variation in the amplitude values is small and has been included in the total systematic error. We fix the values of the mass and central width of ρ' in the fit; if these parameters are allowed to vary, the fit becomes unstable.

To estimate the goodness-of-fit for each model, we generate 40 Monte Carlo samples with the matrix element averaged over the neutrino direction. Each sample is generated with parameters obtained in the fit to the data and the number of events in each sample is approximately equal to that observed in the data. The goodness-of-fit is estimated as a fraction of samples where $-2Ln\mathcal{L}$ exceeds that in the data.

Integrated amplitudes with statistical and systematic errors, as well as the confidence levels of the fits for the four chosen models, are listed in Table IV. The calculation of the systematic errors is explained in the following section. Projections of the fits on various mass combinations are shown in Figs. 8-10.

Models 3 and 4 provide the best description of the data. Both these models are dominated by $\omega\pi$ and $a_1\pi$ with small additional contributions of the $\sigma\rho$, $f_0\rho$ or non-resonant $\rho\pi\pi$ channels. Submass projections for Models 3 and 4 are almost identical, and we show only those for Model 3.

TABLE IV.

Fit results for various models. R_i is defined as: $R_i = \mathcal{B}_i/\mathcal{B}(\tau^- \rightarrow 2\pi^-\pi^+\pi^0\nu_\tau)$, e.g., $R_{a_1\pi} = \mathcal{B}(\tau^- \rightarrow (a_1\pi)^-\nu_\tau)/\mathcal{B}(\tau^- \rightarrow 2\pi^-\pi^+\pi^0\nu_\tau)$.

Model	Integrated amplitudes	Sum of amplitudes	Goodness-of-fit
Model 1	$R_{\rho^0\pi^-\pi^0} = 0.11 \pm 0.01 \pm 0.02$ $R_{\rho^-\pi^-\pi^+} = 0.19 \pm 0.02 \pm 0.04$ $R_{\rho^+\pi^-\pi^-} = 0.23 \pm 0.02 \pm 0.04$ $R_{\omega\pi} = 0.40 \pm 0.02 \pm 0.05$ $R_{3\pi\pi^0} < 0.06$ at 95% CL	$0.93 \pm 0.04 \pm 0.08$	15%
Model 2	$R_{\omega\pi} = 0.38 \pm 0.02 \pm 0.02$ $R_{a_1\pi} = 0.43 \pm 0.02 \pm 0.02$	$0.81 \pm 0.03 \pm 0.03$	< 5%
Model 3	$R_{\omega\pi} = 0.38 \pm 0.02 \pm 0.01$ $R_{a_1\pi} = 0.49 \pm 0.02 \pm 0.02$ $R_{\sigma\rho} = 0.01 \pm 0.02 \pm 0.01$ $R_{f_0\rho} = 0.01 \pm 0.01 \pm 0.01$	$0.89 \pm 0.03 \pm 0.03$	20%
Model 4	$R_{\omega\pi} = 0.39 \pm 0.02 \pm 0.01$ $R_{a_1\pi} = 0.50 \pm 0.03 \pm 0.01$ $R_{\rho^0\pi^-\pi^0} = 0.01 \pm 0.01 \pm 0.01$ $R_{\rho^-\pi^-\pi^+} = 0.02 \pm 0.03 \pm 0.01$ $R_{\rho^+\pi^-\pi^-} = 0.01 \pm 0.01 \pm 0.01$	$0.93 \pm 0.04 \pm 0.02$	20%

The presence of a non-resonant $3\pi\pi^0$ contribution does not improve the goodness-of-fit in the $\omega\pi$ - $\rho\pi\pi$ -non-resonant- $3\pi\pi^0$ model, and we set an upper limit on the non-resonant contribution shown in Table IV. We also ignore the non-resonant $3\pi\pi^0$ component in the

two other models.

F. Systematic errors

To estimate systematic biases and errors for every model, we generate 40 Monte Carlo samples with amplitudes obtained from the fit to the data and then fit them to the chosen parameterization of the hadronic current. Each sample is mixed with simulated background events in the proportion expected from the data. We integrate the results of each simulation to estimate necessary corrections and systematic errors for each of the amplitudes. Biases of the reconstructed amplitude values are shown in Table IV. Errors are determined as root mean squares of the parameter fluctuations.

The total systematic error also includes uncertainty due to the choice of the parameters of ρ' . We use PDG [15] values for the masses and widths of the ρ and ρ'' mesons and vary the ρ' parameters within the errors obtained in the fit described in Section IV. We also switch to a smaller mass of ρ' [11]: $M_{\rho'} = 1370 \text{ MeV}/c^2$. The results appear to have very little sensitivity to the choice of the parameters for ρ' .

All contributions to the systematic error are added in quadrature. Systematic biases for the components of the hadronic current are shown in Table V.

TABLE V.

Systematic biases for the hadronic current components. Systematic bias is defined as $\delta_i = (R_i^{\text{reconstructed}} - R_i^{\text{generated}})/R_i^{\text{generated}}$.

Model	Systematic bias δ_i
Model 1	$\delta_{\rho^0\pi^-\pi^0} = (+4.0 \pm 3.8)\%$
	$\delta_{\rho^-\pi^-\pi^+} = (-7.6 \pm 3.8)\%$
	$\delta_{\rho^+\pi^-\pi^-} = (+2.3 \pm 2.6)\%$
	$\delta_{\omega\pi} = (+2.5 \pm 2.6)\%$
	$\delta_{3\pi\pi^0} = (+1.2 \pm 9.0)\%$
Model 2	$\delta_{\omega\pi} = (+1.0 \pm 2.5)\%$
	$\delta_{a_1\pi} = (-2.0 \pm 2.5)\%$
Model 3	$\delta_{\omega\pi} = (+1.0 \pm 2.5)\%$
	$\delta_{a_1\pi} = (-2.0 \pm 2.6)\%$
	$\delta_{\sigma\rho} = (0.0 \pm 14.0)\%$
Model 4	$\delta_{f_0\rho} = (+1.0 \pm 16.0)\%$
	$\delta_{\omega\pi} = (+1.0 \pm 2.5)\%$
	$\delta_{a_1\pi} = (-2.0 \pm 2.5)\%$
	$\delta_{\rho^0\pi^-\pi^0} = (1.0 \pm 23.0)\%$
	$\delta_{\rho^-\pi^-\pi^+} = (-0.0 \pm 15.0)\%$
	$\delta_{\rho^+\pi^-\pi^-} = (-2.5 \pm 33.0)\%$

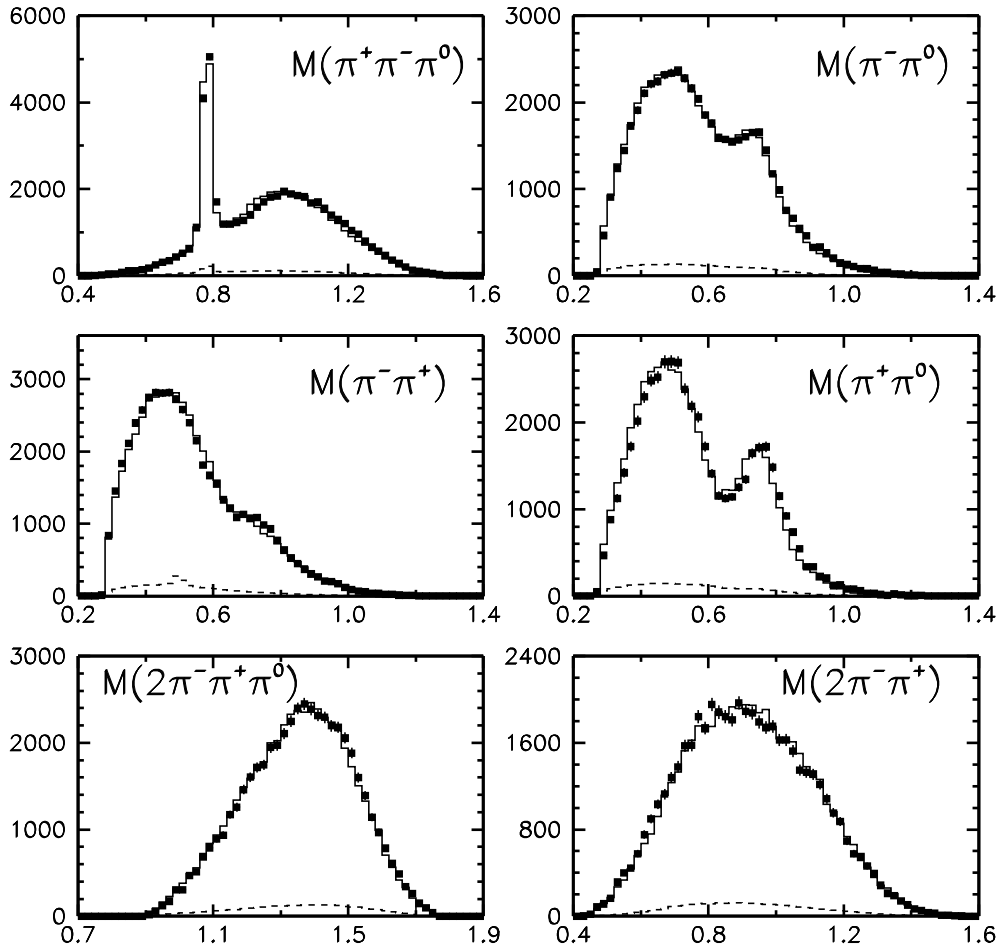


FIG. 8. Comparison between fits and data distributions for the $\omega\pi$, $\rho\pi\pi$ and non-resonant $3\pi\pi^0$ model. The horizontal axis is given in units of GeV/c^2 . Solid squares represent the data, solid line represents the nominal fit, and the dashed line represents the parameterized background.

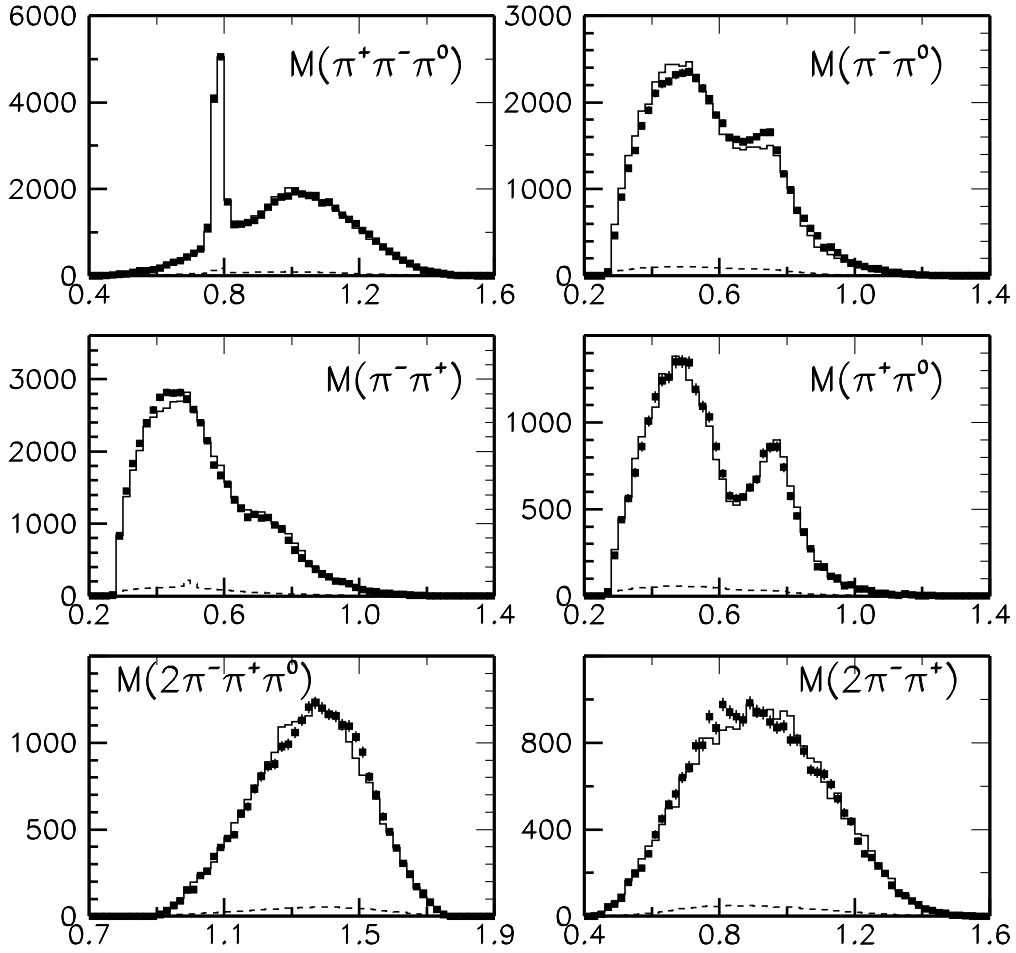


FIG. 9. Comparison between fits and data distributions for the $\omega\pi$ and $a_1\pi$ model. The horizontal axis is given in units of GeV/c^2 . Solid squares represent the data, solid line represents the nominal fit, and the dashed line represents the parameterized background.

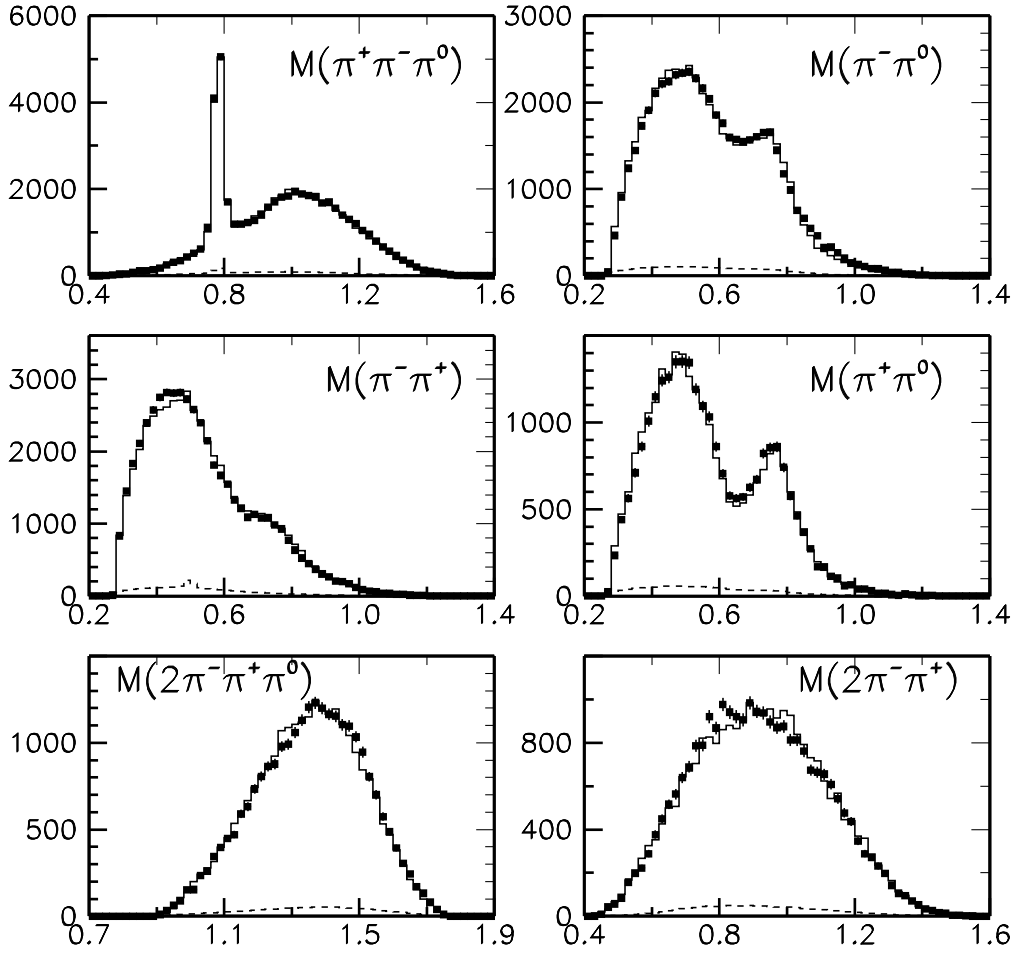


FIG. 10. Comparison between fits and data distributions for the $\omega\pi$, $a_1\pi$, $\sigma\rho$ and $f_0\rho$ model. The horizontal axis is given in units of GeV/c^2 . Solid squares represent the data, solid line represents the nominal fit, and the dashed line represents the parameterized background.

G. Comparison with similar analyses

A recent analysis by the ALEPH Collaboration [4] assumes $\omega\pi$ and non-resonant $\rho\pi\pi$ contributions and uses a simplified fit to the submass projections without assigning systematic errors. This analysis by ALEPH gives the following amplitudes: $R_{\rho^0\pi^-\pi^0} = 0.11$, $R_{\rho^-\pi^-\pi^+} = 0.20$, $R_{\rho^+\pi^-\pi^-} = 0.22$, and $R_{\omega\pi} = 0.40$. Predictions from the chiral perturbation theory [23] for the same model give: $R_{\rho^-\pi^-\pi^+} = 0$, $R_{\rho^+\pi^-\pi^-}/R_{\rho^0\pi^-\pi^0} = 2$. These results can be also compared with the ‘‘standard mix’’ expectations: $R_{\rho^0\pi^-\pi^0} = 0.28$, $R_{\rho^-\pi^-\pi^+} = 0.27$, $R_{\rho^+\pi^-\pi^-} = 0.08$, and $R_{\omega\pi} = 0.30$.

H. CVC test

The CVC hypothesis relates the weak charged hadronic current in the τ lepton decay to the isovector part of the electromagnetic current. Thus, the spectral function (5) can be related [16] to the cross-section for $e^+e^- \rightarrow 4\pi$ as:

$$V^{3\pi\pi^0}(q) = \frac{q^2}{4\pi^2\alpha^2}\sigma_{e^+e^- \rightarrow 4\pi}(q) . \quad (31)$$

Therefore, the resonant structure of the hadronic final state in the decay $\tau \rightarrow 3\pi\pi^0\nu_\tau$ should be comparable to that in the reactions $e^+e^- \rightarrow 2\pi^+2\pi^-$ and $e^+e^- \rightarrow \pi^+\pi^-2\pi^0$ in the energy range corresponding to the τ mass. The only expected difference is due to the fact that the $\omega\pi$ final state is not accessible in the all charged final state. A recent analysis of the CMD-2 data [25] shows clear dominance of the $a_1\pi$ component in the four charged pion final state and of the $a_1\pi$ together with the $\omega\pi$ components in the 2 charged and 2 neutral pion mode.

A plot comparing the $3\pi\pi^0$ and $\omega\pi$ spectral functions in the decay $\tau \rightarrow 3\pi\pi^0\nu_\tau$ with the corresponding cross-sections measured by the CMD-2 group [26] is shown in Fig. 11. Our results are in excellent qualitative agreement and support the CVC hypothesis.

VIII. CONCLUSIONS

The large data sample of $\tau \rightarrow 3\pi\pi^0\nu_\tau$ decays collected by the CLEO II experiment allowed for a detailed study of the resonance decomposition and structure functions of the $3\pi\pi^0$ final state. The analysis indicates dominance of the $\omega\pi$ and $a_1\pi$ contributions which is in good agreement with theoretical expectations based on the CVC hypothesis and Chiral Lagrangian calculations. At the same time, with the present statistics, other models can provide satisfactory descriptions of the existing resonant structure. The goodness-of-fit is slightly higher for the models with a dominating $a_1\pi$ contribution, though the $a_1\pi$ channel alone does not reproduce the observed non- ω contribution precisely. The mass and width of the ρ' resonance have been extracted from the fit to the $\tau \rightarrow \omega\pi\nu_\tau$ spectral function, and a new upper limit on the non-vector current contribution to this spectral function of 5.4% at 90% CL has been obtained.

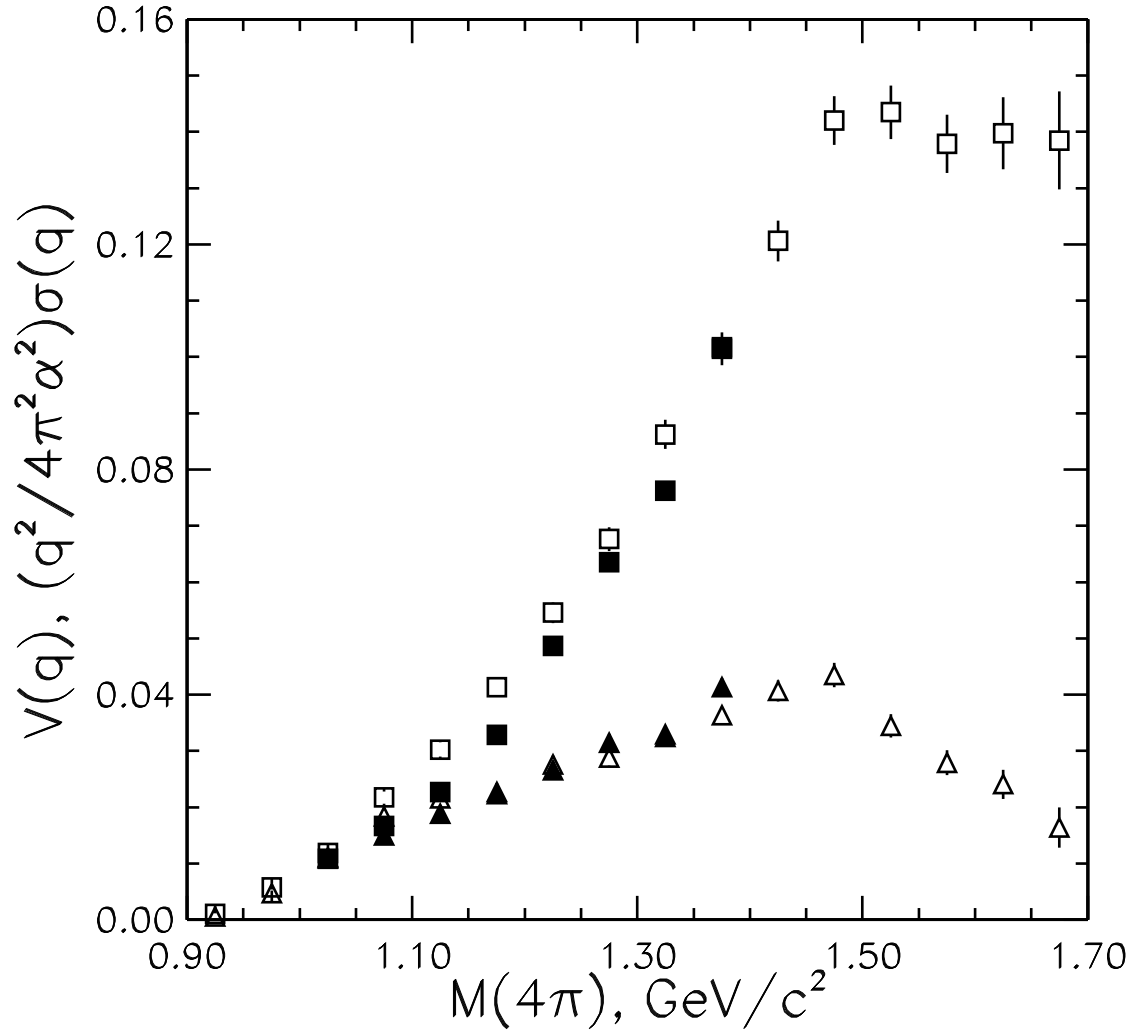


FIG. 11. Comparison of $V^{3\pi\pi^0}(q)$ and $V^{\omega\pi}(q)$ measured in this analysis with the corresponding cross-sections measured by CMD-2. Squares represent the full four-pion spectrum, and triangles represent the $\omega\pi$ component. Our results are shown with open symbols, and the results obtained by CMD-2 are shown with filled symbols.

IX. ACKNOWLEDGMENTS

We gratefully acknowledge the effort of the CESR staff in providing us with excellent luminosity and running conditions. J.R. Patterson and I.P.J. Shipsey thank the NYI program of the NSF, M. Selen thanks the PFF program of the NSF, M. Selen and H. Yamamoto thank the OJI program of DOE, J.R. Patterson, K. Honscheid, M. Selen and V. Sharma thank the A.P. Sloan Foundation, M. Selen and V. Sharma thank the Research Corporation, F. Blanc thanks the Swiss National Science Foundation, and H. Schwarthoff and E. von Toerne thank the Alexander von Humboldt Stiftung for support. This work was supported by the National Science Foundation, the U.S. Department of Energy, and the Natural Sciences and Engineering Research Council of Canada.

REFERENCES

- [1] H. Albrecht *et al.* (ARGUS Collaboration), Phys. Lett. **B 185**, 223 (1987).
- [2] P. Baringer *et al.* (CLEO Collaboration), Phys. Rev. Lett. **59**, 1993 (1987).
- [3] H. Albrecht *et al.* (ARGUS Collaboration), Phys. Lett. **B 260**, 259 (1991).
- [4] D. Buskulic *et al.* (ALEPH Collaboration), Z. Phys. **C 74**, 101 (1997).
- [5] J.H. Kuhn and A. Santamaria, Z. Phys. **C 48**, 445 (1990).
- [6] J.H. Kuhn and E. Mirkes, Z. Phys. **C 56**, 661 (1992).
- [7] R. Decker and E. Mirkes, Z. Phys. **C 57**, 495 (1993).
- [8] B.A. Li, Phys. Rev. **D 58**:097302, (1998).
- [9] S. I. Eidelman and V. N. Ivanchenko, Nucl. Phys. B (Proc.Suppl.) **55C**, 181 (1997).
- [10] R. Barate *et al.* (ALEPH Collaboration), Z. Phys. **C 76**, 15 (1997).
- [11] J. Urheim, Nucl. Phys. B (Proc. Suppl.) **55C**, 359 (1997).
- [12] Y. Kubota *et al.* (CLEO Collaboration), Nucl. Instr. and Meth. **A 320**, 66 (1992).
- [13] J. Alexander *et al.* (CLEO Collaboration), Phys. Rev. **D56**, 5320 (1997).
- [14] R. Decker, Z. Phys. **C 36**, 487 (1987).
- [15] C. Caso *et al.* (Particle Data Group), The European Physical Journal **C**, vol. **3**, number 1-4, (1998).
- [16] Y. S. Tsai, Phys. Rev. **D 4**, 2821 (1971).
- [17] S. Weinberg, *Phys. Rev.* 112, 1375 (1958).
- [18] S. I. Dolinsky, Phys. Lett. **B 174**, 453 (1986).
- [19] S. U. Chung, O.I. Dahl, J. Kirz and D.H. Miller, Phys. Rev. **165**, 1491 (1968).
- [20] KORALB (v.2.1) S. Jadach and Z. Was, Comput. Phys. Commun. **36**, 191 (1985); **64**, 267 (1991); **85**, 453 (1995). TAUOLA (v.1.5) S. Jadach, J. H. Kühn and Z. Was, Comput. Phys. Commun. **64**, 275 (1991); **70**, 69 (1992); **76**, 361 (1993).
- [21] J. Bartelt *et al.* (CLEO Collaboration), Phys. Rev. Lett. **76**, 4119 (1996).
- [22] R. Balest *et al.* (CLEO Collaboration), Phys. Rev. Lett. **75**, 3809 (1995).
- [23] R. Fisher, J. Wess and F. Wagner, Z. Phys. **C 3**, 313 (1980).
- [24] N.A. Törnqvist, Z. Phys. **C 68**, 647, (1995).
- [25] R. R. Akhmetshin *et al.*, hep-ex/990424v2, (1999).
- [26] A.E. Bondar, S.I. Eidelman, A.I. Milstein and N.I.Root, hep-ph/9907283, (1999).

**APPENDIX A: HADRONIC CURRENT FOR THE DECAYS $\tau \rightarrow A_1\pi\nu_\tau$, $\tau \rightarrow \sigma\rho\nu_\tau$
AND $\tau \rightarrow F_0\rho\nu_\tau$**

Expressions for the hadronic current for τ decays into the four pion final state via $a_1\pi$, $\sigma\rho$ and $f_0\rho$ channels are derived under the assumption that the τ decays into an intermediate vector resonance $\tilde{\rho}$: $\tau \rightarrow \tilde{\rho}\nu_\tau$, which consecutively decays into the shown channels. The vector boson $\tilde{\rho}$ has quantum numbers $I(J^{PC}) = 1(1^{--})$, and its spectral function, in accordance with Eqn. (29), is simulated as mixture of ρ and ρ' resonances and a phase space contribution. Assuming isospin conservation and enforcing Bose symmetry, one obtains the following expressions for the form factors f_i^μ in the decay $\tau^- \rightarrow 2\pi^-\pi^+\pi^0\nu_\tau$:

$$f_{a_1\pi}^\mu = T^{\mu\nu}(q) \times \left[\begin{aligned} & T_{\nu\kappa}(Q_1)BW_{a_1}(Q_1^2) \left[BW_\rho((q_1 + q_2)^2)(q_1 - q_2)^\kappa + BW_\rho((q_1 + q_4)^2)(q_1 - q_4)^\kappa \right] \\ & - T_{\nu\kappa}(Q_2)BW_{a_1}(Q_2^2) \left[BW_\rho((q_1 + q_3)^2)(q_1 - q_3)^\kappa + BW_\rho((q_2 + q_3)^2)(q_2 - q_3)^\kappa \right] \\ & - T_{\nu\kappa}(Q_3)BW_{a_1}(Q_3^2) \left[BW_\rho((q_1 + q_3)^2)(q_1 - q_3)^\kappa + BW_\rho((q_3 + q_4)^2)(q_4 - q_3)^\kappa \right] \end{aligned} \right]; \quad (\text{A1})$$

$$f_{\sigma\rho}^\mu = T^{\mu\nu}(q) \times \left[\begin{aligned} & BW_\sigma((q_1 + q_2)^2)BW_\rho((q_3 + q_4)^2)(q_4 - q_3)_\nu \\ & + BW_\sigma((q_1 + q_4)^2)BW_\rho((q_2 + q_3)^2)(q_2 - q_3)_\nu \end{aligned} \right]; \quad (\text{A2})$$

where

$$\begin{aligned} q_1 &:= \text{four-momentum of } \pi^+; \\ q_2 &:= \text{four-momentum of } \pi_1^-; \\ q_3 &:= \text{four-momentum of } \pi^0; \\ q_4 &:= \text{four-momentum of } \pi_2^-; \end{aligned} \quad (\text{A3})$$

$$\begin{aligned} q &= q_1 + q_2 + q_3 + q_4; \\ Q_1 &= q_1 + q_2 + q_4; \\ Q_2 &= q_1 + q_2 + q_3; \\ Q_3 &= q_1 + q_3 + q_4; \end{aligned} \quad (\text{A4})$$

and $T^{\mu\nu}(x)$ denotes the projection operator:

$$T^{\mu\nu}(x) = -g^{\mu\nu} + \frac{x^\mu x^\nu}{x^2}. \quad (\text{A5})$$

The expression for the τ decay into four pions via the $f_0\rho$ channel is identical to Eqn. (A2) with the mass of f_0 substituted instead of the mass of σ .